Cell growth dilutes YAP/TAZ influencing its subcellular distribution and phenotypic heterogeneity

Ian Jones[1], Patricia Pascual Vargas[1], Maria Arias-Garcia[1], Julia Sero[2], Chris Bakal[1]

1. Chester Beatty Laboratories, Division of Cancer Biology, Institute of Cancer Research, 237 Fulham Road, London SW3 6JB, UK
2. Institute for Mathematical Innovation, Department of Life Sciences, University of Bath, Claverton Down, Bath, BA2 7AY, UK

Corresponding authors: chris.bakal@icr.ac.uk, ian.jones@icr.ac.uk

Lead contact: ian.jones@icr.ac.uk

Abstract

Protein concentrations are not constant across cell sizes; many dilute or concentrate in response to growth. Through quantitative analysis of ~400,000 single cells across ten cell breast epithelial cell lines (including tumour and non-tumour cells), we show that the cytoplasmic and total concentrations of YAP/TAZ, decreases as a function of cell size in G1 and G2. Degradation of YAP/TAZ alone could not explain this phenomenon. Near S-Phase, YAP/TAZ was synthesised in a ploidy and size dependent manner. Theoretical modelling of YAP/TAZ concentration distributions demonstrated the rate of dilution with cell size relates to YAP/TAZ heterogeneity across the population. YAP/TAZ dilution in the cytoplasm was largely robust to perturbations in Rho GTPase and LATS1/2 signalling, whereas the YAP/TAZ nuclear cytoplasmic (n/c) ratio, was not. Alterations to the n/c ratio following perturbation were more commonly driven by cytoplasmic dilution rather than nuclear enrichment.

Together, this work reveals how size scaling phenomena may influence the subcellular distribution of transcription factors, and more generally, relates protein dilution to the emergence of non-genetic heterogeneity in cell populations.

Introduction:

Cellular protein concentrations often do not scale with cell size, with many diluting or concentrating as the cell grows (*1–6*). Particularly striking examples are RB1 and WHI5, inhibitors of the G1/S transition in mammalian and *S. pombe* cells (*7*, *8*), which are titrated against proteins that promote G1/S, CCND1 and CLN3. The ratio of these factors is thus, a mechanism through which cell size may inform the proliferation-quiescence decision (*9*, *10*). Size-scaling phenomena has a been observed to influence biosynthetic signalling, DNA repair and the stress response leading to an increasing belief that cell size, and the associated DNA/cytoplasm ratio, may mechanistically underpin cell senescence (*1*, *6*, *11*, *12*).

In normal cells, sequestration of YAP/TAZ proteins in the cytoplasm renders them transcriptionally inactive. In the cytoplasm YAP/TAZ functions as a core regulatory component of the CTNNB1 destruction complex (*20*, *21*) and is thought to influence mitotic processes (*22*). Nuclear translocation of YAP/TAZ is triggered by soluble, mechanical, and geometrical cues (*23–31*). For example, changes in cell shape and size can activate YAP/TAZ (*24*). The coupling of YAP/TAZ dynamics to cell shape provides a mechanism that allows cells to position themselves during development, or to sense and respond to disruption in tissue structures (*13*, *15*, *32*, *33*). Changes in cell shape and size are coupled to the signalling dynamics of Rho GTP Exchange Factors (RhoGEFs), Rho GTPase Activating Proteins (RhoGAPs) and their downstream effector Rho GTPases regulate YAP/TAZ translocation (*28*, *33–39*).

As potent proliferative and growth regulators, YAP and TAZ (hereafter referred to as YAP/TAZ) regulate cell, tissue and organ size (*13–15*). While increases in tissue and organ size have been historically associated with the hyperproliferative effects of YAP/TAZ amplification, the mechanistic basis of YAP/TAZ's effects on cell size remains elusive, though a recent study identified potential cell autonomous and non-autonomous pathways of size regulation (*16*). Furthermore, YAP/TAZ activity may influence cell size through the manipulation of cell mechanics, compressing/expanding the cytoplasm through its control over cytoskeletal effectors and processes. Recent works point to substrate stiffness and adherence controlling cell volume via a feedback system with YAP/TAZ (*17*, *18*), and cell size being manipulated by actomyosin contraction, expelling water from the cell (*19*).

YAP/TAZ are activation is associated many cancer subtypes, especially in breast cancer (*40*, *41*)). YAP/TAZ activation promotes several clinically relevant behaviours such as survival, proliferation, drug resistance, the Epithelial-to-Mesenchymal Transition (EMT), migration, and invasion (*24*, *30*, *42*, *43*). Moreover, the evolved drug resistance of many cancers is due to dysregulation of YAP/TAZ activity (*44*–*50*).

Here we show through quantitative analysis of ~400,000 single cells, from ten cell lines, that the cytoplasmic YAP/TAZ concentration, decreases as a function of cell size in G1 and G2. YAP/TAZ synthesis is dramatically upregulated near S-Phase in a size and ploidy dependent manner such to maintain an approximately constant YAP/TAZ concentration across generations. Through mathematical modelling of YAP/TAZ dilution through sequential division cycles, we found that the severity of size-scaling relates to the variance of the YAP/TAZ concentration distribution of the cell lines, implicating YAP/TAZ dilution in the emergence of YAP/TAZ heterogeneity across cell populations. Conducting a screen of an siRNA library targeting the majority of human RhoGEFs and RhoGAPs, we found YAP/TAZ scaling was robust to perturbation that affect Rho GTPase activation, suggesting that scaling, and thus the development of phenotypic heterogeneity, stems from a physical process. Interestingly, increases in YAP/TAZ n/c ratio were found to be driven by a decrease in the cytoplasmic (and total) YAP/TAZ concentration rather than an increasing nuclear fraction, potentially implicating YAP/TAZ size-scaling in the regulation of transcription.

Together this study reveals the size-scaling nature of YAP/TAZ, and evidences more generally that the phenomenon contributes to non-genetic heterogeneity in cancers.

Results

YAP1 concentration decreases with increasing cell size:

It is becoming increasingly evident that the concentration of signalling proteins is a critical factor in the dynamics of signalling pathways. We reasoned that as YAP/TAZ are conserved effectors of cell geometry (*24*), their cellular protein concentration, as influenced by cell shape and size, could influence their activity.

We quantified 114 morphological and intensity features describing the size and shape of the cells, and the distribution and abundance of YAP/TAZ and (F) actin, first in ~ 30,000 single cells from nine breast epithelial cell lines (**Supp.Table 1**). We modelled the concentrations of these proteins (integrated intensity/cell area, mean intensity) as power law relationships with cell area, $[C] = aA^b$, such that we could define a 'scaling factor', 'b', for each species. In a log-log plot, 'b' is given as the gradient and log(a) is the y-intercept. Negative values of 'b' correspond to the dilution of the protein with increasing cell size, 0, linear scaling, and positive values, concentration of the protein with increasing size. Fitting 'a' and 'b' values to each cell lines F-actin concentration profiles, we observed linear scaling between cell size and F-actin (b ranging from -0.2 to 0.2, **Fig.1A, Supp.Table 2**) as observed in previous studies (*9*, *10*). However, when applying the same analysis to (whole cell) YAP/TAZ concentration, we observed, for all cells lines, a clear sub-scaling relationship between cell size and YAP/TAZ concentration (b ~ -0.35 - -0.65), indicating that YAP/TAZ dilutes as a cell gets larger (**Fig.1A, Supp.Table 3**).

To investigate the decrease in YAP/TAZ concentration with cell size, we also analysed the abundance (integrated whole cell intensity, rather than mean) -size relationship and observed that YAP/TAZ abundance increases with cell size, but not at a rate sufficient to maintain a constant concentration (b ~ 0.6). Total YAP/TAZ increased with size at all sizes implying continued synthesis; an increase in cell size is thus necessary to enable the dilution as YAP/TAZ degradation is not overcoming synthesis. (**Fig.1B, Supp.Table 4, Supp.Fig.1**). F-actin exhibited 1:1 abundance scaling. (**Supp.Fig.1, Supp.Table 5**). By comparing YAP/TAZ concentration across the 3-fold size range of our cell lines, we noticed no clear dependence of YAP/TAZ concentration with size (**Fig.1C**). This indicted that the relationship between size and YAP/TAZ concentration may be confined to the size changes within a cell cycle rather than absolute size.

Together these data reveal the nature sub-scaling of YAP/TAZ concentration, is dependent on reduced scaling of YAP/TAZ abundance in the background of an expanding cell size.

YAP/TAZ concentration, but not scaling, is sensitive to DNA-content:

Noticing that YAP/TAZ concentration decreased with size within, but not between lines, we hypothesised that the observed sub-scaling of YAP may relate to cell cycle processes. To investigate this, within each line we binned cells based on their DNA content (integrated Hoechst intensity, one of the previous measured 114 features). Bin sizes were constrained such that each bin centroid represents double the value of the preceding bins. Conducting the previous analysis on each DNA 'bin' within each line, we noticed that while the mean YAP/TAZ concentration at any given size increased for each doubling of the cell DNA (each DNA content 'bin', ~1.3-1.6 factor increase) (**Supp.Table 3, Fig.1D**), the scaling factor 'b' showed no obvious DNA dependence. We enacted the same analysis for the F-actin concentration and noticed no relationship between 'b' or mean concentration and DNA content (**Fig.1E, Supp.Table 2**).

Importantly, YAP/TAZ abundance showed a consistent positive scaling factor (~0.4-0.6) across all DNA contents, further indicating that it is insufficient synthesis of YAP/TAZ in the background of an expanding cell that is underpinning the sub scaling of YAP/TAZ, not just degradation (**Supp.Table 4/5 ,Supp.Fig 1/2/3**).

As YAP/TAZ dilutes during 'G1' and 'G2' (first and second DNA 'bins'), the DNA-dependent regeneration of YAP/TAZ at S-phase is vital to the maintenance of a constant generational YAP/TAZ concentration.

YAP/TAZ scaling rate is a function of cell size:

While we observed clear sub-scaling behaviour when investigating the average scaling factor of YAP/TAZ with cell size, we were interested in how this extended to the case where the scaling factor 'b' is treated as a continuous function of cell size, b(A). We extracted b(A) by taking the logarithmic derivative of YAP/TAZ concentration with respect to the cell area:

$$b(A) = \frac{dlog_2([YAP/TAZ])}{dlog_2(A)} \qquad equ\ (1$$

Strikingly, no cell line exhibited a constant scaling factor. Scaling factors ('b') tended to be lower in small cells and steadily decreased with increasing cell size (within a cell line); however, in several lines, this relationship would reverse at larger sizes, with further increases in area leading to weaker sub-scaling. This extended to both

the G1 and G2 populations. Remarkably, in a subset of our lines (eg. HCC1954, MDA-MB-231), YAP/TAZ concentration even positively scaled with cell size at small sizes. Although, this effect was limited to G1 cells (**Fig.2A**) implying the existence of an area-dependent scaling trigger.

To understand how significant size-variable scaling is to the functioning of the cell, we calculated the range of scaling factors that occur over the most common size "bands", which we define here as the mean G1/G2 sizes +/- 1 std deviation. Calculating this for the G1 cells, we observed that 5/9 of our cell lines exhibited only a modest variation in the scaling factor within this size constraint (stddev = 0.03-0.08). However, the remainder showed far more extreme variations (stddev = 0.14-0.17) leading to an approximate 2-fold change in scaling factor 'b' across the size range (**Fig.2B**). The mean scaling rate was approximately constant across cell lines (-0.4 - -0.5). In the G2 group, the variation in scaling rate increased (std = 0.10-0.18) for all lines, and the mean scaling rate significantly decreased for only a subset (**Fig.2C**). Thus, the YAP/TAZ scaling factor varies within relevant size ranges and should not be considered a constant.

We also investigated how the fold difference in YAP/TAZ concentration between 'G1' and 'G2' cells, *K*, varied with cell size. In most (7/9) of our cell lines, K was found to decrease with increasing cell size; at small sizes (mean size – 2std deviations) taking values between 1.3-1.6, and at larger sizes (mean size + 2std deviations), 1-1.3 (**Fig.2D**).

Together, these data show that the scaling of YAP/TAZ with cell size is not static but changes dynamically with cell size within relevant size ranges in both G1 and G2 cells. This size-dependence extended to the fold-change across DNA-contents, 'K', suggesting that the size at which a cell passes the G1/S checkpoint informs the scaling and production of YAP/TAZ across subsequent cell cycle stages and potentially, generations.

The YAP/TAZ nuclear/cytoplasmic increases with cell size through cytoplasmic dilution rather than nuclear concentration:

The nuclear to cytoplasmic ratio (N/C, defined as (integrated nuclear intensity * Cell Area) / (nuclear area *integrated whole cell intensity)) of YAP/TAZ reflects its transcriptional activity and is sensitive to both mechanical and biochemical stimuli.

For example, phosphorylation of YAP/TAZ by the LATS1/2 kinases, downstream elements of the Hippo signalling cascade, sequesters YAP in the cytoplasm, while inhibitory phosphorylations on the LATS1/2 kinases promote nuclear entry(*30*, *31*, *43*, *51*). Furthermore, YAP/TAZ nuclear translocation has been associated with the activation of mechanically sensitive elements of focal adhesions, such as Talin1 and structural alterations to the nuclear pore complexes(*24*, *28*, *52*, *53*). Having observed a sub-scaling relationship between YAP/TAZ and cell size, we were interested in how this related to the nuclear translocation of YAP/TAZ.

We quantified the N/C ratio of YAP/TAZ at the single cell level, for each cell line. Interestingly, YAP/TAZ ratio increased with increasing cell size, exhibiting the opposite relationship to (whole cell) YAP/TAZ concentration. This extended to the N/C ratios relationship with DNA content, where the mean YAP/TAZ ratio, decreased across each DNA 'bin'. We noted that 'b', the scaling factor between cell area and N/C, remained unchanged across DNA contents for all cell lines (**Fig.3A, Supp.Table 6**).

We next investigated the scaling of the nuclear concentration of YAP/TAZ with both the nuclear and cell areas. At small nuclear sizes (128um2 – 256um^2), the nuclear YAP/TAZ concentration was observed to strongly super scale (b= ~1 - 4) in 2n G1 cells. Beyond this, the concentration was approximately invariant to further increases in nuclear size. Increases in the DNA content, however, did increase nuclear YAP/TAZ, but not sufficiently to maintain the same YAP/TAZ ratio across DNA bins (**Fig.3B/D, Supp.Table 7**). Considering instead scaling with the cell area, we again observed an increase in nuclear YAP/TAZ with increasing DNA content; however, not all lines exhibited super-scaling behaviour at low cell sizes, as was the case at low nuclear sizes. Interestingly, those which did, were the same as those which showed the greatest variance in 2n G1 scaling rate of total YAP/TAZ and exhibited positive scaling rates at small sizes (**Fig.3C/E, MDA-MB-231, MDAMB157, JIMT1, hs578T**).

Together, these data suggest that while the cytoplasmic pool of YAP/TAZ is sensitive to cell size, the nuclear YAP/TAZ concentration, is regulated independently. YAP/TAZ n/c ratio increasing with cell size is not driven by an increasing nuclear fraction, but rather a decreasing cytoplasmic fraction in these cell lines.

An increased nuclear YAP/TAZ concentration correlates with a reduction in the YAP/TAZ scaling factor:

We noticed that lines exhibiting super-scaling behaviour in their nuclear YAP/TAZ concentrations at small cell sizes were those with the most variable scaling factors. To investigate this, we began by assuming a linear relationship between the scaling factor 'b' and the logarithm of the nuclear YAP/TAZ concentration:

$$b(A) = \frac{d\,log_2([Y])}{d\,log_2(A)} = \mu\, log_2([Y]_N) + c \qquad equ(2$$

Where 'μ' and c are constants to be determined through fitting to the experimentally determined b(A) and Yn. As b(A) and Yn vary with size only at very small sizes, when fitting to this equation, we considered only cells meeting the criterion $A_c < \langle A \rangle - \sigma$, where '$\langle A \rangle$' is the mean cell area and 'σ' is the standard deviation. This avoided the greater density of points at a constant 'b' and 'Yn' from skewing the calculation. We used equ.2 to calculate the expected scaling rate at each cell area and found excellent agreement with that measured (**Fig.4A**). Importantly, while an increase in nuclear YAP/TAZ leads to a decrease in scaling factor, a decrease in YAP/TAZ leads to an increase in scaling factor (**see SUM149 and MDAMB157 F4A**). This suggests that the effect is not driven by a correlate of YAP/TAZ import but by a correlate of the nuclear fraction itself.

This effect did not extend across lines; higher nuclear YAP/TAZ concentrations did not lead to lower scaling factors. Instead scaling factors were more associated with higher YAP/TAZ ratios. The direction of causality is unclear, but it is plausible that higher scaling factors induce greater ratios by virtue of reducing the cytoplasmic YAP/TAZ fraction (**Fig.4B/C**). Together, this suggests that the correlation between the nuclear YAP/TAZ concentration and scaling factor may emerge from a co-dependence on an unseen cryptic variable rather than any direct effect of the nuclear YAP/TAZ concentration, however, we cannot yet exclude the possibility of a negative feedback mechanism.

YAP/TAZ scaling persists across cell cycle phases

Although we observed that YAP/TAZ concentration/ scaling behaviour was sensitive to the DNA content of the cell, implying a cell cycle effect, we sought to more

rigorously investigate the relationship between cell cycle progression and YAP/TAZ concentration. We stained MCF10A cells for YAP/TAZ, PCNA and CCNA2 and trained a linear classifier to distinguish G0, G1, S and G2 cells through 110 CCNA2 and PCNA intensity features (methods) across ~ 20,000 single cells. Conducting a scaling analysis within each stage, we observed that the negative size-YAP/TAZ concentration scaling is preserved across all stages besides G0 (**Supp.Fig.4**). Moreover, by binning the cells by area and calculating the mean YAP/TAZ concentration in each stage, we observed that the YAP/TAZ concentration increases from G1 to G2 and that smaller cells exhibit a greater YAP/TAZ concentration at each stage, further corroborating the previous analysis (**Supp.Fig.4**).

Interestingly, this result implies that cell cycle progression is required to invoke the size-scaling of YAP/TAZ, as cell cycle exit (G0) attenuated the phenomena; however, cell growth during the cycle is nevertheless necessary for YAP/TAZ dilution, as the abundance increases across all size bins implying a constant synthesis.

YAP/TAZ abundance, concentration and N/C ratio scaling are insensitive to cell crowding

Cell size and YAP/TAZ activation have previously been associated with cell crowding and contact inhibition (*15*). In our cell lines, cell area negatively correlated with neighbour fraction (NF), raising the possibility that the observed size-YAP/TAZ scaling was cryptically driven by the NF (**Supp.Fig.5**). To investigate this, we first quantified the extent to which YAP/TAZ scaled with NF, noticing a strong positive association at high NF's (0.4 -1), in accordance with the area correlation. However, when clustering the cells on NF, and conducting a scaling analysis between YAP/TAZ concentration and cell area within each NF group, we observed no change in mean YAP/TAZ or 'b' across clusters, while the YAP/TAZ area scaling persisted (**Supp.Fig.5**). We conducted the same analysis for YAP/TAZ abundance and N/C ratio, noting the same effect, with the exception that MCF10A's YAP/TAZ N/C ratio exhibited a NF sensitivity (**Supp.Fig.5**). From these data, we concluded it is the NF's influence on cell area that is driving the NF-YAP scaling relationship rather than any direct effect of NF on YAP/TAZ in these lines.

Integration of YAP/TAZ size-scaling and stochastic cell division fosters YAP/TAZ heterogeneity:

The previous analyses are consistent with a scheme by which a constant generational amount of YAP is maintained through dilution in G1, synthesis at S/G2, dilution through the subsequent G2, and then inheritance of YAP/TAZ by daughter cells (A dilution-synthesis-dilution, or DSD, scheme). Theoretically, we assume a two-stage growth system. To understand how YAP/TAZ scaling effects the YAP/TAZ concentration distribution, we integrated a DSD model with a simple cell cycle system (exhibiting adder size behaviour) (*6*). This model assumes linear dependencies between cell area and the probability to advance in cell cycle stage and cell area and growth rate. The cell area probability distribution under these constraints is given as a hypo exponential function:

$$F(A,S,n) = \mathcal{F}^{-1}\left(\prod_{i=1}^{n} \mathcal{F}(G(A,S,n))\right) \quad equ\ (3$$

$$G(A,S,n) = \frac{\alpha}{\ln(2)\,k}\sum_{i=1}^{S}\left[\prod_{i\neq j}\frac{1}{1+2^{j-i}}\right]\frac{ne^{-\frac{n\alpha A}{2^{i}\ln(2)k}}}{2^{i}} \qquad equ\ (4$$

Where: ‘Ad’ is the cell area at division, ‘α’ is a proportionality constant between Ad and cell cycle advancement probability, ‘k’ a proportionality constant between Ad and growth rate, ‘S’ is the number of divisions that have occurred, and ‘n’ is the number of cell cycle ‘stages’ per division. ‘$\mathcal{F}(f(x))$’ denotes the Fourier transform of f(x), and $\mathcal{F}^{-1}$, the inverse. (**See methods (calculating area distributions) and supplemental information for details).**

To ensure the applicability of this model, we fit equ.6 to the (G2) cell area distributions of our cell lines using a two-stage system and found good agreement (methods). Here ‘stage’ refers to the number of growth stages in a cycle (**Fig.5B**). Indeed, the CVs of the distributions lie well within the predicted bounds of a two-stage system (CV = 1/sqrt(3n). For n = 2, ~0.4 < CV < ~0.57) (**Supp.Table 7**) (*6*).

Expressing the ‘cell cycle advancement time’ (time spent in each cycle stage, CCA) distribution in terms of the dilution factor ‘D’ (D = 1/exp(b*k*t), where ‘b’ is the scaling

factor, k the proportionality constant between size and growth rate and t is time) gives (**F5C**) (see supplemental information):

$$P(D) = \frac{-\ln(1-\alpha A_d)\,(1-\alpha A_d)^{\frac{-\ln D}{bk}}}{Dbk} \qquad equ\ (5$$

Where: Ad is the cells size at division and 'α' is proportionality constant (**Supp.Info**). As two dilution events happen in sequence, we were interested in the product distribution of P(D) and a second dilution event, denoted as F(z) (**Fig.5D**):

$$F(z) = \frac{-\ln(z)\ln(1-\alpha A_d)^2\,(1-\alpha A_d)^{-\frac{\ln(z)}{bk}}}{b^2k^2z} \qquad equ\ (6$$

Where z is the product of two random 'D' variables distributed according to equ.(8). For simplicity we considered the two sequential dilution events to be identical, such that the cell grows equally across G1 and G2 and exhibit the same scaling behaviour. From F(z) we could calculate the coefficient of variation (std dev/mean):

$$CV = \frac{\sigma}{\mu} \approx \frac{\sqrt{\left(\frac{\alpha A_d}{\alpha A_d + 2bk}\right)^2 - \left(\frac{\alpha A_d}{\alpha A_d + bk}\right)^4}}{\left(\frac{\alpha A_d}{\alpha A_d + bk}\right)^2} \qquad equ\ (7$$

Which approximately linearly scales with 'b' for 0 < b < 1 (**Fig.5E**); note we have expanded the mean and variance about a = 0 to obtain equ.10 (α values do not exceed 10^-5) (methods). Correlating average scaling factors ((bs1+bs2)/2) against the CV of YAP/TAZ intensity distributions, we observed a strong negative trend for 7/9 of our cell lines (**Supp.Fig.6**).

It is important to note that average 'b' values are not the only source of YAP/TAZ variance in this system; differences in size regulation and the area dependence of 'K' and 'b' all contribute to YAP/TAZ variability. Indeed, the MDA-MB-231 and JIMT1 cell lines, those with high scaling rates (b ~ -0.54) but comparatively low YAP/TAZ variance (CV ~ 0.37), have more homogenous size distributions than most of the other cell lines (**Supp.Table 8,** CV~0.48) and are some of the few to exhibit an approximately constant 'K' value (**Fig.2D**) providing an explanation for their departure from a linear scaling-variance relationship.

To capture the concentration distribution of YAP/TAZ, we simulated equ.9 across multiple generations (**Fig.5F**) (methods). Parameter (Q) values (bs1, bs2, K) were taken from the size-Q curves for each cell line. Comparing the predicted distributions to those measured, we observed excellent agreement showing that, in these cell lines, the concentration distribution of YAP/TAZ can be explained by the interplay of size-scaling and stochastic cell division (**Fig.5G**).

Size scaling factors are closely related to the cell-to-cell variation of YAP/TAZ concentration. In conjunction with the apparent size dependence of YAP/TAZ synthesis at S/G2, YAP/TAZ size-scaling could function as a powerful engine of non-genetic heterogeneity in breast cancer.

YAP/TAZ scaling behaviour drives increasing nuclear/cytoplasmic ratios following gene depletion:

YAP/TAZ nuclear translocation has been shown to be regulated by numerous upstream pathways, especially those involving Rho family GTPases. In both normal and cancer cells, Rho GTPases appear to regulate YAP/TAZ translocation 'directly' – i.e. by activating kinases such as PAK which may phosphorylate YAP and regulate binding to 14-3-3 proteins (*54*, *55*). Rho GTPases can also affect YAP/TAZ translocation indirectly, by regulating cytoskeleton organization which can in turn influence translocation(*23*, *24*, *38*, *47*). To determine if Rho signalling regulates the YAP protein levels, and the scaling rates of YAP/TAZ throughout the cell cycle, we used the OnTargetPlus siRNA library to systematically deplete 82 RhoGEFs, 67 GAPs and 19 Rho GTPases, across ~ 300,000 LM2 and MDA-MB-231 cells (The LM2 cell line is a metastatic derivative of MDA-MB-231). This let us investigate whether the size dependence of YAP/TAZ could be modulated.

Conducting a scaling analysis on the untreated cells (LM2 and MDA-MB-231 cells) (n ~ 80,000), we observed the same whole cell YAP/TAZ concentration sub-scaling behaviour as in the prior analyses (b = ~0.35), although super-scaling behaviour at small cell sizes was clearer. Similarly, the nuclear concentration remained approximately constant with size, leading to an increasing YAP/TAZ n/c ratio driven by cytoplasmic dilution. Applying the same analysis to the KD states, strikingly, very few materially affected the size-YAP/TAZ scaling factor (**Fig.6A**). Thus, the scaling of

YAP/TAZ levels to size appears rarely affected by perturbations which affect size, morphology, or Rho GTPase pathway activation.

As expected, the gene depletions did affect the n/c ratio (*28*). For example, depletion of genes such as SPATA13, RALBP1 and BCR increased average YAP/TAZ concentrations/ n/c ratios for any given cell sizein MDA-MB-231 cells. Investigating more deeply, we constructed partial least squares regression (PLSR) models which predicted YAP/TAZ concentration and ratio in control cells as functions of 114 measured morphological and intensity features (methods) (**Supp.Fig.7/8**). Calculating variable importance to projection (VIP) scores from the model, we observed that cell area (and associated correlates e.g. Nuclear area, eccentricity etc. most contributed to the prediction of YAP/TAZ concentration and n/c ratio (VIP scores > 1 are considered major contributors to the model (**Supp Info**)). We applied this model to all treatment conditions (siRNA knockdowns) finding that, even under perturbation, the size-YAP/TAZ n/c ratio and concentration relationship persists (**Supp.Fig.7/8**). Thus, while many siRNA are affecting the YAP/TAZ n/c ratio, often they are doing so through manipulation of cell morphology and dilution of cytoplasmic (and total) YAP/TAZ, rather than increasing the nuclear fraction. These included genes canonically associated with increased cell size, including ECT2 and RACGAP1, known to induce cytokinetic failures and polyploidisation when depleted (*56*).

Using this system, we could also investigate genes that disrupt the coupling between YAP/TAZ and size; those which are most poorly predicted by the model are those which most perturb the relationship between YAP/TAZ and cell morphology. The clearest ‘hits’ across both cell lines included YAP itself, the YAP regulatory kinases LATS1 and LATS2, as well as RHOA, HMHA1 and PIK3R2. Unique to LM2 cells were ARHGAP33 and STARD13 whilst SOS2 and ITSN2 perturbed the relationship only in MDA-MB-231 cells (**Fig.6B**).

Focusing on MDA-MB-231 cells, LATS1/2 and HMHA1 interestingly exhibited a very similar behaviour to that captured by the model, in that they exhibited an increased cell area and YAP/TAZ ratio, a decreased whole cell YAP/TAZ concentration and approximately unchanged nuclear YAP/TAZ concentration. However, these KDs led to an increase in YAP/TAZ ratio beyond what would be expected from an increase in

size alone, in accordance with LATS1/2's role in the nuclear – cytoplasmic shuttling of YAP/TAZ (**Fig.6C**). Thus, we conclude these genes affect the cytoplasmic levels of YAP/TAZ both via control of morphology, size and signalling.

This phenomenon was not universal, however; several KD states altered the YAP/TAZ ratio independently of cell area, such as PIK3R2 and ITSN2 (**Fig.6C**). Interestingly, the reduction in YAP/TAZ ratio observed in these cases was nevertheless associated with a loss of cytoplasmic rather than nuclear YAP/TAZ concentration, indicating that an increase in cell area is not the only way to achieve a reduction in cytoplasmic YAP/TAZ concentration (e.g. Increased degradation). These genes could be involved in directly regulating YAP/TAZ translocation.

Of our 'hit' genes that increased YAP/TAZ n/c and cell area, only RHOA depleation led to a decrease in YAP/TAZ ratio, driven by a canonical reduction in nuclear, rather than total, YAP/TAZ concentration (**Fig.6C**). It is unclear whether RHOA depleation reduces the nuclear translocation of YAP/TAZ, leads to an increase in YAP/TAZ synthesis per cell size, such to offset the effect of size scaling on the mean YAP/TAZ concentration, or whether it decouples cell area from cell volume, leading to an anomalously high spread area skewing the result. Indeed, such an effect may underpin the behaviour of PIK3R2/ITSN2 KD.

Together, these data show that while YAP/TAZ scaling is remarkably robust to genetic perturbations, many such perturbations appear to act through size scaling to exert their effects on the YAP/TAZ ratio. For example, ECT2, HMHA1, DOCK5 and LATS1/2. (**See the supplemental information for a comprehensive list of KD YAP/TAZ ratios, concentrations, and model errors**).

Discussion:

Here we have shown that YAP/TAZ are sub-scaling molecules in breast epithelial cells; specifically, diluting in G1, undergoing a surge in synthesis near S-phase and diluting again in G2. This is not unique to YAP/TAZ; seminal work on size-scaling phenomena showed that RB1 (and the associated Whi5 in yeast) exhibits extremely similar behaviour. However, unlike YAP/TAZ, RB1 is not continually synthesised throughout the cell cycle/across sizes ($b_{abundance}$ ~ 0.15 vs 0.4-0.6 for YAP/TAZ) (*3*, *9*, *10*). The concentration of RB1 is, therefore, more directly controlled by changes in

cell volume, befitting of its putative role as a size-sensor, whereas the YAP/TAZ concentration is complicated by biosynthetic regulation. Given that [YAP/TAZ] is not a sole function of cell size, we believe it unlikely that YAP/TAZ size scaling serves to measure cell volume. Indeed, with many hundreds of proteins being shown to scale across cell lines (*1*, *5*, *6*, *11*, *12*), size-scaling behaviour should not be considered sufficient evidence of a size-measurement system.

YAP/TAZ are known to be directly regulated by the Hippo signalling pathway, which serves to phosphorylate and sequester YAP/TAZ in the cytoplasm, blunting their transcriptional activity (*26*, *28–30*, *40*). This system appears influenced by dynamical changes to the cytoskeleton and adhesion, with pharmacological inhibition of ROCK/myosin activity and genetic perturbation of adhesion components severely limiting the nuclear translocation of YAP/TAZ (*37*, *38*). Here, we show that the nuclear translocation of YAP/TAZ, or rather the YAP/TAZ N/C ratio is also a function of cell size, with larger cell sizes leading to higher YAP/TAZ ratios. However, nuclear YAP/TAZ remained at an approximately constant concentration across cell sizes in all cell lines, besides exhibiting 'super-scaling' behaviour at very small cell areas. This suggested that the nuclear concentration of YAP/TAZ quickly achieves a maximum, or equilibrium condition in these lines. The origin of this effect is unclear, but may stem from constitutive activation, indeed many cancer tissues, particularly breast, are known to exhibit constitutively active YAP/TAZ (*26*, *51*, *57*, *58*), or a result of cell culturing on stiff materials (*52*, *53*). Regardless, this indicated that the increasing N/C ratio of YAP/TAZ was not due to an increase in nuclear YAP/TAZ concentration, but rather through a decrease in the cytoplasmic (and total) concentration.

YAP/TAZ is known to engage in a feedback system, inhibiting its own synthesis and partly instigating YAP/TAZ degradation in the cytoplasm (*59*). This may participate in the falling cytoplasmic concentration of YAP/TAZ, as across multiple lines we observed that an increase in nuclear YAP/TAZ concentration coincided with a subsequent decrease in cytoplasmic scaling. Wee noted that YAP/TAZ abundance scales positively with cell size across all sizes, and so degradation alone could not be driving the sub-scaling behaviour of YAP/TAZ. Furthermore, LATS1/2 knockdown did not materially affect the size-scaling of YAP/TAZ suggesting that the phenomenon occurs independently of hippo signalling (*27*, *40*, *58*), which opposes

the traditional view of the YAP/TAZ feedback system. This is consistent with the observation that cell crowding did not affect YAP/TAZ concentration or activation beyond its effect on cell area, as contact inhibition is thought to at least partly act through the sequestration of YAP/TAZ in the cytoplasm (*15*). This does not exclude a role for nuclear translocation of YAP/TAZ in size-scaling however, as YAP/TAZ have been implicated in the direct regulation of cell volume through the manipulation of mechanical signalling events and cytosolic pressure (*14*, *17–19*). Equally, YAP/TAZ may be engaging in a feedback system through a yet undiscovered system.

It remains unclear whether there is a causal connection between the nuclear translocation of YAP/TAZ and YAP/TAZ size scaling or if the relationship is driven by a cryptic hidden variable. Indeed, this study uses cell area as a proxy for cell volume and recent studies have shown that the area-volume relationship is not linear during cell spreading (*17*). As the smallest cells in our dataset will be those having recently divided, this effect may relate to the more positive scaling factors we observe at smaller cell sizes as the same gain in cell area does not lead to the same gain in cell volume at small and large areas. However, the same study also shows that the relationship becomes linear at larger sizes, explaining why the scaling factor tends to a constant value with increasing size (*17*). This also provides an explanation for the correlation with the nuclear YAP/TAZ concentration and scaling factor, as cell spreading is known to induce the nuclear translocation of YAP/TAZ(*24*, *38*).

By constructing linear models of YAP/TAZ concentration and ratio, and systematically knocking down a set of RhoGEF/GAPs in MDA-MB-321 and LM2 cells, we identified proteins that decoupled YAP/TAZ activity and cell morphology when depleted. These did not materially affect the YAP/TAZ scaling factor, however, YAP/TAZ scaling was found crucial to the increase in YAP/TAZ n/c ratio associated with many knockdown states including LATS1/2. The nuclear-cytoplasmic ratio has been shown to be more closely related to the transcriptional output of several signalling systems, such as the MAPK and WNT pathways, than the absolute nuclear concentration (*60–62*) suggesting that YAP/TAZ size scaling may influence its transcriptional output. Although, it remains unclear whether this phenomenon extends to YAP/TAZ activity.

Our theoretical model, integrating stochastic cell division with YAP/TAZ size scaling, revealed that more severe protein-size scaling results in a greater variance in the proteins concentration distribution; This may have drastic consequences for the cytoplasmic functions of YAP/TAZ; for example, YAP/TAZ has been shown to influence the spindle assembly checkpoint, potentially through its interactions with BUBR1 (*22*). Moreover, cytoplasmic YAP/TAZ is known to be a core component of the CTNNB1 destruction complex (*20*, *21*). As YAP/TAZ and CTNNB1 co-operate as transcription factors in the nucleus (*63*, *64*), this suggests that the cytoplasmic dilution of YAP/TAZ may also indirectly influence its nuclear activity in accordance with the putative importance of the YAP/TAZ nuc/cyto ratio (*60–62*).

Together, these data show that in breast cancer, YAP/TAZ can dilute as the cell increases in size. This drives an increase in the YAP/TAZ n/c ratio potentially influencing transcriptional activity. As size-scaling promotes variance in concentration distributions, YAP/TAZ scaling may act as an engine driving the development of non-genetic heterogeneity in breast cancers where YAP/TAZ is constitutively nuclear.

Methods:

Cell Culture

Cell lines were maintained in standard culture conditions (DMEM+10% FBS, vessel: Corning® Primaria™ 25cm² Rectangular Canted Neck Cell Culture Flask with Vented Cap, PN: 353808). Passage was carried out using 0.25% trypsin-EDTA (GIBCO) followed by centrifugation (1000 rpm, 4 min) and resuspension in complete medium. Cell counting was performed using Countess automated cell counter with trypan blue exclusion (Thermo).

Immunostaining:

Samples were fixed in freshly prepared 4% PFA/PBS for 15 minutes. Slides were subsequently permeabilized with 0.25% Triton/PBS for 10 mins and blocked with 0.5% BSA/0.02% glycine/PBS for 30 minutes. Primary antibodies were introduced via the same solution in a 1:1000 dilution and left on for 1 hour. The slides were washed with PBS and the same was carried out for the secondary antibodies (kept in

the dark to avoid bleaching). Hoechst stain was added post-secondary (1:500) to stain DNA as was phalloidin to stain actin.

Image Acquisition and Feature Extraction

Image acquisition was performed using an Opera Cell: Explorer-automated spinning disk confocal microscope. 20 fields of view were imaged in each well (PerkinElmer, PhenoPlate 384-well, black, optically clear flat-bottom, tissue-culture treated, PN: 6057302). Cell segmentation was performed using Acapella software (PerkinElmer). Nuclei were segmented using the Hoechst channel (405-450) and cell bodies defined by the tubulin signal (568-603). Geometric features measured include: the area of all subcellular regions; the length, width, and elongation (length/ width) of the cell and nucleus, cell and nuclear roundness and nucleus area/cytoplasm area.

Scaling analysis

We conducted k-means clustering on the integrated Hoescht intensity of each cell line against nuclear area across k = 1:8. k was calculated using the elbow method and augmented with the additional constraint that cluster centroids should be separated by a factor of 2^x, where x = 1:k. This way, the first cluster approximates 2n G1, the second 2n G2/4n G1 and so on. The YAP/TAZ – size relationship in each DNA-cluster was treated as a power law such that:

$$[Y] = aA^b \qquad equ\ (8$$

Where; [Y] represents YAP/TAZ concentration, ‘A’, cell area and a and b are constants. The scaling factor, ‘b’ and ‘log(a)’ was extracted by conducting a linear fit on:

$$\log[Y] = \log a + \mathrm{b}\log A \qquad equ\ (9$$

Which results from simple manipulation of equ.11 . The factor by which ‘a’ increases across DNA groups is trivially retrieved by:

$$\log_2 a_{n+1} - \log_2 a_n = x \ , \ \frac{a_{n+1}}{a_n} = 2^x \qquad equ\ (10$$

Examining the logarithmic derivative of [Y], we noticed that ‘b’ was not constant across the entire size range captured in our populations, although was over an 8-fold

size difference about the mean. To avoid this complicating our analysis, we conducted the linear fits on the data within three standard deviations of the mean. Linear fitting, clustering and data handling was conducted in the MATLAB R2019b (Mathworks) environment.

Calculating cell area distributions:

Cell area distributions were derived from a simple adder system we published in a previous study (*6*). Briefly, we considered the probability of a cell advancing to the next cell cycle stage at any given time, P, and the cells growth rate, β, as proportional to the area at which it divided in the previous cycle:

$$P = \alpha A_d \ , \qquad \beta = kA_d \qquad equ\ (11$$

Where 'α' and 'k' are proportionality constants. From these two rules, it can be shown that in each cell cycle stage, the cell gains a random amount of mass drawn from a size-invariant exponential distribution centred on k/α, R(A), resulting in adder-like behaviour:

$$R(A) = \lambda e^{-\lambda A}, \quad \lambda = \frac{-\ln(1-\alpha A_d)}{A_d \mathrm{k} \ln(2)} \approx \frac{\alpha}{\ln(2)\,k} \qquad equ\ (12$$

The division area distribution, H(A), results from the convolution of the birth distribution B(A) with R(A) 'n' times, where n is the number of cell cycle stages. Assuming symmetrical cell division, the subsequent B(A) (in the next cycle), is given as H(2A). This is then again convolved with R(A)… etc. This results in a hypo-exponential distribution of general form:

$$F(x,n) = \sum_{i=1}^{S}\left[\prod_{i\neq j}\frac{\lambda_j}{\lambda_j+\lambda_i}\right]\lambda_i e^{-\lambda_i x} \quad equ(13$$

Substituting our values for a one -stage cycle system:

$$F(A,S) = \sum_{i=1}^{S}\left[\prod_{i\neq j}\frac{\frac{\alpha}{2^j\ln(2)\,k}}{\frac{\alpha}{2^j\ln(2)\,k}+\frac{\alpha}{2^i\ln(2)\,k}}\right]\frac{\alpha}{2^i\ln(2)\,k}e^{-\frac{\alpha A}{2^i\ln(2)\,k}}$$

$$F(A,S) = \frac{\alpha}{\ln(2)\,k}\sum_{i=1}^{n}\left[\prod_{i\neq j}\frac{1}{1+2^{j-i}}\right]\frac{ne^{-\frac{n\alpha A}{2^i\ln(2)\,k}}}{2^i} \qquad equ(14$$

The n-stage distribution is obtained by first substituting λ for nλ:

$$G(A,S,n) = \frac{\alpha}{\ln(2)\,k}\sum_{i=1}^{S}\left[\prod_{i\neq j}\frac{1}{1+2^{j-i}}\right]\frac{ne^{-\frac{n\alpha A}{2^i\ln(2)k}}}{2^i} \qquad equ(15$$

And convolving G(A,S,n) with itself 'n' times:

$$F(A,S,n) = \mathcal{F}^{-1}\left(\prod_{i=1}^{n}\mathcal{F}(G(A,S,n))\right) \qquad equ(16$$

Where '$\mathcal{F}(c)$' denotes the Fourier transform of 'c' and '$\mathcal{F}^{-1}(c)$' the inverse. Here we have leveraged the convolution theorem to expression the convolution as a multiplication in Fourier space.

For calculation, the initial cell area distributions are considered a delta function centred on '$\ln(2)$k'/'α' (the mean of R(A)). Every generation, the area distribution is convolved with the mass-gain distribution, R(A), 'n' times, computed by performing an inverse Fourier transform on the product of the two distributions respective Fourier transforms. This produces the division area distribution, Ad(A), which must be transformed to Ad(2A) to capture the effects of cell division. We perform this by setting Ab(Ax) = Ad(Ai) + Ad(Ai+1) , where 'I' = x_n-x_{n-1} for all x, where Ab denotes the birth size distribution. This is then convolved with the gain distribution as before to generate the next division distribution and so on until a desired number of generations has been reached. For each we calculated the Kullbeck-Liebler divergence between the experimental and simulated data to assess model error. For discrete probability distributions defined on the same probability space, X, the Kullback–Leibler divergence from P to Q is**:**

$$D_{KL}(P\|Q) = \sum_{x\in X} P(x)\,log_{10}\left(\frac{P(x)}{Q(x)}\right) \qquad equ\ (17$$

Model fitting was conducted within the commercial MATLAB R2019b (Math Works) software's machine learning toolbox.

Calculation of YAP/TAZ concentration distributions:

We computed the dilution factor distribution for an initial size condition, constrained such that the cell begins the simulation at its ‘expected size’ within our, 2-stage, adder proliferation model framework:

$$Ad = < A > \ , \ \ \alpha = \frac{w}{Ad} \ \ , \qquad k = \frac{w}{4 \ln 2} \qquad equ\ (18$$

Where ‘w’ is an arbitrary constant. These parameters are used to compute an initial dilution factor distribution:

$$P(D) = \frac{-\ln(1-\alpha A_d)\,(1-\alpha A_d)^{\frac{-\ln D}{bk}}}{Dbk} \qquad equ\ (19$$

From which we compute the product distribution (assuming identical cell cycle stages):

$$F(z) = \int_z^1 P(D) P\left(\frac{z}{D}\right)\frac{1}{D}\, dD \qquad equ\ (20$$

$$F(z) = \frac{-\ln(z)\ln(1-\alpha A_d)^2\,(1-\alpha A_d)^{-\frac{\ln(z)}{bk}}}{b^2k^2z} \qquad equ\ (21$$

Where we assume that the cell grows approximately equal amounts in G1 vs G2. We then draw from this distribution, obtaining a dilution factor ‘d’, by passing a uniformly distributed random number through the inverse of G(z), defined as:

$$G(z) = \int_0^1 F(z)dz \qquad equ\ (22$$

We multiply the initial YAP concentration by ‘K*d’ to generate the starting YAP concentration for the next cycle. ‘K’ is taken from the size-K curve experimentally measured. From this, we also calculated the size change needed to generate ’d’ as:

$$\Delta A = \frac{A_d}{2b}\ln\left(\frac{1}{d}\right) \qquad equ\ (23$$

From which we trivially update Ad:

$$A_{d_{n+1}} = \frac{1}{2}A_{d_n} + \Delta A \qquad equ\ (24$$

This now facilitates re-calculation of P(D), F(z)… etc. for the next generation and the cycle is repeated for 10 generations to generate one sample YAP concentration for the cell line. The process is repeated 1000 times to generate a YAP/TAZ concentration distribution for each line which is compared to the experimentally determined YAP/TAZ intensity distributions via the KBL divergence.

To calculate the coefficient of variation of F(z), we first derived the mean:

$$\langle F(z)\rangle = \int_0^1 zF(z)dz = \frac{\ln(1-\alpha A_d)^2}{(\ln(1-\alpha A_d)-bk)^2} \approx \left(\frac{\alpha A_d}{\alpha A_d + bk}\right)^2 \qquad equ\ (25$$

Where we have expanded about alpha = 0. The variance is given as:

$$\langle\langle F(z)\rangle\rangle = \int_0^1 z^2 F(z)dz - \mu^2$$

$$\approx \left(\frac{\alpha A_d}{\alpha A_d + 2bk}\right)^2 - \left(\frac{\alpha A_d}{\alpha A_d + bk}\right)^4 \qquad equ\ (26$$

Where we have made the same simplification. From these we obtain the coefficient of variation as:

$$CV \approx \frac{\sqrt{\left(\frac{\alpha A_d}{\alpha A_d + 2bk}\right)^2 - \left(\frac{\alpha A_d}{\alpha A_d + bk}\right)^4}}{\left(\frac{\alpha A_d}{\alpha A_d + bk}\right)^2} \qquad equ\ (27$$

PLSR and hit detection:

Regression analyses were conducted with the MATLAB (MathWorks) environment using the plsregress function from the machine learning toolbox, Partial least squares regression was selected as the method to help mitigate the influence of co-linearity in the predictor dataset. Model components were selected through 10-fold cross validation using the elbow method on the mean square error as a function of component number. All 114 shape features were mean centralised prior to model construction. Models were built from control data and applied to the combined knockdown-control state. Fit quality was assessed through the r-squared metric. Linear models (predicted vs observed) were visualised through the ‘dscatter’ function. Z scores were calculated for the difference between observed and

predicted YAP/TAZ ratios/abundances and the increase/decrease from the mean YAP/TAZ ratio/abundances. Knockdown 'Hits', those which decoupled were selected from this analysis as knockdown states achieving an average Z-score > 2 (two standard deviations from the mean).

Feature Importance to PLSR models:

The influence a feature has on a model was estimated through 'Variable importance to projection' (VIP) scores calculated as:

$$VIP_j = \sqrt{\frac{\sum_{f=1}^{F} w_{jf}{}^2 \cdot SSY_f \cdot J}{SSY_{total} \cdot F}} \qquad equ\ (28$$

wjf is the weight value for j variable and f component and SSYf is the sum of squares of explained variance for the fth component and J number of X variables. SSYtotal is the total sum of squares explained of the dependent variable, and F is the total number of components. Features with a VIP score greater than 1 were taken as major drivers of the model.

RNAi screening methodology

40nl (0.08pmol) of siRNA from an ONTARGETPlus human siRNA RhoGEF/GAP and Rho GTPase library (stock concentration of 20µM, Dharmacon) were arrayed using the acoustic liquid handler Echo 550 prior to transfection and kept at -80°C. All siRNAs were arrayed in duplicate per plate and each plate was arrayed in duplicate resulting in a total of 4 plates. Pre-stamped siRNA plates were thawed at room temperature for 30 minutes prior to use. 5µl of Opti-MEM® Reduced Serum Media were then added per well followed by 5µl of RNAiMax reagent (Invitrogen) and Opti-MEM® mix in a 1:125 ratio. Plates were spun down at 1000 rpm for 1 min and incubated at room temperature for 20 mins. Cells were then seeded at a concentration of 33000 cells/ml (1000 cells per well~ 1.5 million cells per screen, 4 wells per siRNA, 4000 cells/siRNA per screen) in 30µl DMEM supplemented with 12.8% FBS, 1.28% penicillin/streptomyocin (10% FBS and 1% penicillin/streptomyocin final) to account for the 10 µl of mix already present in the well, resulting in a total volume of 40µl per well. Automated handling of plates on the Cell::Explorer robot station was carried out using the PlateWorks software (Perkin

Elmer). Plates were fixed 48 hours later with 8% warm formaldehyde in PBS (final concentration 4%) for 15 minutes and permeabilised with 0.1% Triton-X-100 in PBS for 10 minutes. Cells were then blocked in 2% BSA in PBS for 2 hours. All antibody incubations were performed in solution containing 0.5% BSA, 0.01% Triton-X-100 dissolved in PBS in a 1:1000 ratio, with the first primary antibody being added overnight at 4°C and the rest being incubated at room temperature for 1.5 hours. Plates were washed 3x with PBS between every step using a Microplate Washer (BioTek). Antibodies were added sequentially to prevent cross reactivity. Antibodies used were: mouse YAP/TAZ (Santa Cruz Biotechnologies, cat # sc-101199), rat α - tubulin (Bio-Rad, cat # MCA77G), AlexaFluor 647 goat anti-mouse (Life Technologies, cat # A21235), AlexaFluor 647 goat anti-rat (Life Technologies, cat # A11077), phalloidin (Invitrogen, cat # A12379). Finally Hoechst (Sigma Aldrich, cat # 33258) was added for 15 minutes, and after washing, cells were left in PBS and plates were sealed. Cells were imaged using an automated Opera Quadrupule Enhanced High Sensitivity (QEHS) spinning-disk confocal microscope (Perkin Elmer) with 20x air lens. 28 fields of view were imaged per well. Cells were plated at increasing densities on columns 1, 2, 23 and 24 to be able to account for density dependent effects. SUM159 and hs578t were plated at a density of 67000 cells/ml (2000 cells/well) and 50000 cells/ml (1500 cells/well) respectively (~ 2.5 million cells per screen, 4 wells per siRNA, 1500 to 2000 cells/well, 6000 - 8000 cells/siRNA per screen).

Contributions

I.Jones analysed the data, developed the computational models and with P.Vargus and C.Bakal wrote the manuscript. P.Vargus maintained and imaged the cells and conducted the RNAi screen. J.Sero cooperated on the analysis and the imaging and maintenance of the cells. M.Arias-Garcia optimized the RNAi screening methodology. C.Bakal conceived and designed the research.

Acknowledgments

This work was supported by a Stand Up to Cancer UK Programme Foundation Award from Cancer Research UK to Chris Bakal (C37275/1A20146). We thank Vicky Bousgouni and Lucas Dent for their helpful comments on the manuscript.

Data Availability:

A demonstration of the model and corresponding numerical simulation may be found at: IJICR/Model_demo (github.com)

Image datasets for the cell lines used for morphological profiling are available from: DRYAD: http://dx.doi.org/10.5061/dryad.tc5g4.

Image Data Repository (http://idr-demo.openmicroscopy.org/about, accession number S-BSMS6)

Biostudies database (https://www.ebi.ac.uk/biostudies/studies/S-BSMS6).

Competing Interests

The authors declare no conflict of interest.

References

1. L. Cheng, J. Chen, Y. Kong, C. Tan, R. Kafri, M. Björklund, Size-scaling promotes senescence-like changes in proteome and organelle content. *bioRxiv* (2021).

2. A. A. Amodeo, D. Jukam, A. F. Straight, J. M. Skotheim, Histone titration against the genome sets the DNA-to-cytoplasm threshold for the Xenopus midblastula transition. *Proc Natl Acad Sci U S A*. **112** (2015), doi:10.1073/pnas.1413990112.

3. M. P. Swaffer, J. Kim, D. Chandler-Brown, M. Langhinrichs, G. K. Marinov, W. J. Greenleaf, A. Kundaje, K. M. Schmoller, J. M. Skotheim, Transcriptional and chromatin-based partitioning mechanisms uncouple protein scaling from cell size. *Mol Cell*. **81** (2021), doi:10.1016/j.molcel.2021.10.007.

4. M. C. Lanz, E. Zatulovskiy, M. P. Swaffer, L. Zhang, I. Ilerten, S. Zhang, D. S. You, G. Marinov, P. McAlpine, J. E. Elias, J. M. Skotheim, Increasing cell size remodels the proteome and promotes senescence. *Mol Cell*. **82**, 3255-3269.e8 (2022).

5. G. Yahya, P. Menges, P. S. Amponsah, D. A. Ngandiri, D. Schulz, A. Wallek, N. Kulak, M. Mann, P. Cramer, V. Savage, M. Räschle, Z. Storchova, Sublinear scaling of the cellular proteome with ploidy. *Nat Commun*. **13**, 6182 (2022).

6. I. Jones, L. Dent, T. Higo, T. Roumeliotis, M. Arias Garcia, H. Shree, J. Choudhary, M. Pedersen, C. Bakal, Characterization of proteome-size scaling

by integrative omics reveals mechanisms of proliferation control in cancer. *Sci Adv*. **9** (2023), doi:10.1126/sciadv.add0636.

7. M. Chinnam, D. W. Goodrich, *RB1, Development, and Cancer* (2011), vol. 94.

8. M. Costanzo, J. L. Nishikawa, X. Tang, J. S. Millman, O. Schub, K. Breitkreuz, D. Dewar, I. Rupes, B. Andrews, M. Tyers, CDK activity antagonizes Whi5, an inhibitor of G1/S transcription in yeast. *Cell*. **117** (2004), doi:10.1016/j.cell.2004.05.024.

9. K. M. Schmoller, J. J. Turner, M. Kõivomägi, J. M. Skotheim, Dilution of the cell cycle inhibitor Whi5 controls budding-yeast cell size. *Nature*. **526** (2015), doi:10.1038/nature14908.

10. E. Zatulovskiy, S. Zhang, D. F. Berenson, B. R. Topacio, J. M. Skotheim, Cell growth dilutes the cell cycle inhibitor Rb to trigger cell division. *Science (1979)*. **369** (2020), doi:10.1126/science.aaz6213.

11. G. E. Neurohr, R. L. Terry, J. Lengefeld, M. Bonney, G. P. Brittingham, F. Moretto, T. P. Miettinen, L. P. Vaites, L. M. Soares, J. A. Paulo, J. W. Harper, S. Buratowski, S. Manalis, F. J. van Werven, L. J. Holt, A. Amon, Excessive Cell Growth Causes Cytoplasm Dilution And Contributes to Senescence. *Cell*. **176** (2019), doi:10.1016/j.cell.2019.01.018.

12. M. C. Lanz, E. Zatulovskiy, M. P. Swaffer, L. Zhang, I. Ilerten, S. Zhang, D. S. You, G. Marinov, P. McAlpine, J. E. Elias, J. M. Skotheim, Increasing cell size remodels the proteome and promotes senescence. *bioRxiv* (2021).

13. J. Dong, G. Feldmann, J. Huang, S. Wu, N. Zhang, S. A. Comerford, M. F. F. Gayyed, R. A. Anders, A. Maitra, D. Pan, Elucidation of a Universal Size-Control Mechanism in Drosophila and Mammals. *Cell*. **130** (2007), doi:10.1016/j.cell.2007.07.019.

14. N. A. Perez-Gonzalez, N. D. Rochman, K. Yao, J. Tao, M. T. T. Le, S. Flanary, L. Sablich, B. Toler, E. Crentsil, F. Takaesu, B. Lambrus, J. Huang, V. Fu, P. Chengappa, T. M. Jones, A. J. Holland, S. An, D. Wirtz, R. J. Petrie, K. L. Guan, S. X. Sun, YAP and TAZ regulate cell volume. *Journal of Cell Biology*. **218** (2019), doi:10.1083/JCB.201902067.

15. B. Zhao, X. Wei, W. Li, R. S. Udan, Q. Yang, J. Kim, J. Xie, T. Ikenoue, J. Yu, L. Li, P. Zheng, K. Ye, A. Chinnaiyan, G. Halder, Z. C. Lai, K. L. Guan, Inactivation of YAP oncoprotein by the Hippo pathway is involved in cell contact inhibition and tissue growth control. *Genes Dev*. **21** (2007), doi:10.1101/gad.1602907.

16. D. Mugahid, M. Kalocsay, X. Liu, J. S. Gruver, L. Peshkin, M. W. Kirschner, YAP regulates cell size and growth dynamics via non-cell autonomous mediators. *Elife*. **9** (2020), doi:10.7554/eLife.53404.

17. L. Venkova, A. S. Vishen, S. Lembo, N. Srivastava, B. Duchamp, A. Ruppel, S. Vassilopoulos, A. Deslys, J. M. G. Arcos, A. Diz-Muñoz, M. Balland, J.-F. Joanny, D. Cuvelier, P. Sens, M. Piel, A mechano-osmotic feedback couples cell volume to the rate of cell deformation. *bioRxiv* (2021), doi:10.1101/2021.06.08.447538.

18. K. Xie, Y. Yang, H. Jiang, Controlling Cellular Volume via Mechanical and Physical Properties of Substrate. *Biophys J*. **114** (2018), doi:10.1016/j.bpj.2017.11.3785.

19. M. Guo, A. F. Pegoraro, A. Mao, E. H. Zhou, P. R. Arany, Y. Han, D. T. Burnette, M. H. Jensen, K. E. Kasza, J. R. Moore, F. C. Mackintosh, J. J. Fredberg, D. J. Mooney, J. Lippincott-Schwartz, D. A. Weitz, Cell volume change through water efflux impacts cell stiffness and stem cell fate. *Proc Natl Acad Sci U S A*. **114** (2017), doi:10.1073/pnas.1705179114.

20. C. Chen, D. Zhu, H. Zhang, C. Han, G. Xue, T. Zhu, J. Luo, L. Kong, YAP-dependent ubiquitination and degradation of β-catenin mediates inhibition of Wnt signalling induced by Physalin F in colorectal cancer article. *Cell Death Dis*. **9** (2018), doi:10.1038/s41419-018-0645-3.

21. L. Azzolin, T. Panciera, S. Soligo, E. Enzo, S. Bicciato, S. Dupont, S. Bresolin, C. Frasson, G. Basso, V. Guzzardo, A. Fassina, M. Cordenonsi, S. Piccolo, YAP/TAZ incorporation in the β-catenin destruction complex orchestrates the Wnt response. *Cell*. **158** (2014), doi:10.1016/j.cell.2014.06.013.

22. S. Yang, L. Zhang, X. Chen, Y. Chen, J. Dong, Oncoprotein YAP regulates the spindle checkpoint activation in a mitotic phosphorylation-dependent manner through up-regulation of BubR1. *Journal of Biological Chemistry*. **290** (2015), doi:10.1074/jbc.M114.624411.

23. M. Aragona, T. Panciera, A. Manfrin, S. Giulitti, F. Michielin, N. Elvassore, S. Dupont, S. Piccolo, A mechanical checkpoint controls multicellular growth through YAP/TAZ regulation by actin-processing factors. *Cell*. **154** (2013), doi:10.1016/j.cell.2013.07.042.

24. S. Dupont, L. Morsut, M. Aragona, E. Enzo, S. Giulitti, M. Cordenonsi, F. Zanconato, J. le Digabel, M. Forcato, S. Bicciato, N. Elvassore, S. Piccolo, Role of YAP/TAZ in mechanotransduction. *Nature*. **474** (2011), doi:10.1038/nature10137.

25. J. M. Lamar, P. Stern, H. Liu, J. W. Schindler, Z. G. Jiang, R. O. Hynes, The Hippo pathway target, YAP, promotes metastasis through its TEAD-interaction domain. *Proc Natl Acad Sci U S A*. **109** (2012), doi:10.1073/pnas.1212021109.

26. T. Moroishi, C. G. Hansen, K. L. Guan, The emerging roles of YAP and TAZ in cancer. *Nat Rev Cancer*. **15** (2015), doi:10.1038/nrc3876.

27. D. Pan, The hippo signaling pathway in development and cancer. *Dev Cell*. **19** (2010), , doi:10.1016/j.devcel.2010.09.011.

28. J. E. Sero, C. Bakal, Multiparametric Analysis of Cell Shape Demonstrates that β-PIX Directly Couples YAP Activation to Extracellular Matrix Adhesion. *Cell Syst*. **4** (2017), doi:10.1016/j.cels.2016.11.015.

29. J. E. Sero, H. Z. Sailem, R. C. Ardy, H. Almuttaqi, T. Zhang, C. Bakal, Cell shape and the microenvironment regulate nuclear translocation of NF -κB in breast epithelial and tumor cells . *Mol Syst Biol*. **11** (2015), doi:10.15252/msb.20145644.

30. A. Totaro, T. Panciera, S. Piccolo, YAP/TAZ upstream signals and downstream responses. *Nat Cell Biol*. **20** (2018), , doi:10.1038/s41556-018-0142-z.

31. B. Zhao, X. Ye, J. Yu, L. Li, W. Li, S. Li, J. Yu, J. D. Lin, C. Y. Wang, A. M. Chinnaiyan, Z. C. Lai, K. L. Guan, TEAD mediates YAP-dependent gene induction and growth control. *Genes Dev*. **22** (2008), doi:10.1101/gad.1664408.

32. J. Huang, S. Wu, J. Barrera, K. Matthews, D. Pan, The Hippo signaling pathway coordinately regulates cell proliferation and apoptosis by inactivating Yorkie, the Drosophila homolog of YAP. *Cell*. **122** (2005), doi:10.1016/j.cell.2005.06.007.

33. A. Reginensi, R. P. Scott, A. Gregorieff, M. Bagherie-Lachidan, C. Chung, D. S. Lim, T. Pawson, J. Wrana, H. McNeill, Yap- and Cdc42-Dependent Nephrogenesis and Morphogenesis during Mouse Kidney Development. *PLoS Genet*. **9** (2013), doi:10.1371/journal.pgen.1003380.

34. Z. Diamantopoulou, G. White, M. Z. H. Fadlullah, M. Dreger, K. Pickering, J. Maltas, G. Ashton, R. MacLeod, G. S. Baillie, V. Kouskoff, G. Lacaud, G. I. Murray, O. J. Sansom, A. F. L. Hurlstone, A. Malliri, TIAM1 Antagonizes TAZ/YAP Both in the Destruction Complex in the Cytoplasm and in the Nucleus to Inhibit Invasion of Intestinal Epithelial Cells. *Cancer Cell*. **31** (2017), doi:10.1016/j.ccell.2017.03.007.

35. X. Feng, M. S. Degese, R. Iglesias-Bartolome, J. P. Vaque, A. A. Molinolo, M. Rodrigues, M. R. Zaidi, B. R. Ksander, G. Merlino, A. Sodhi, Q. Chen, J. S.

Gutkind, Hippo-independent activation of YAP by the GNAQ uveal melanoma oncogene through a Trio-regulated Rho GTPase Signaling Circuitry. *Cancer Cell*. **25** (2014), doi:10.1016/j.ccr.2014.04.016.

36. J. K. H. Hu, W. Du, S. J. Shelton, M. C. Oldham, C. M. DiPersio, O. D. Klein, An FAK-YAP-mTOR Signaling Axis Regulates Stem Cell-Based Tissue Renewal in Mice. *Cell Stem Cell*. **21** (2017), doi:10.1016/j.stem.2017.03.023.

37. N. G. Kim, B. M. Gumbiner, Adhesion to fibronectin regulates Hippo signaling via the FAK-Src-PI3K pathway. *Journal of Cell Biology*. **210** (2015), doi:10.1083/jcb.201501025.

38. H. Sabra, M. Brunner, V. Mandati, B. Wehrle-Haller, D. Lallemand, A. S. Ribba, G. Chevalier, P. Guardiola, M. R. Block, D. Bouvard, β1 integrin–dependent Rac/group I PAK signaling mediates YAP activation of Yes-associated protein 1 (YAP1) via NF2/merlin. *Journal of Biological Chemistry*. **292** (2017), doi:10.1074/jbc.M117.808063.

39. G. Sorrentino, N. Ruggeri, V. Specchia, M. Cordenonsi, M. Mano, S. Dupont, A. Manfrin, E. Ingallina, R. Sommaggio, S. Piazza, A. Rosato, S. Piccolo, G. del Sal, Metabolic control of YAP and TAZ by the mevalonate pathway. *Nat Cell Biol*. **16** (2014), doi:10.1038/ncb2936.

40. K. F. Harvey, X. Zhang, D. M. Thomas, The Hippo pathway and human cancer. *Nat Rev Cancer*. **13** (2013), , doi:10.1038/nrc3458.

41. J. G. Tate, S. Bamford, H. C. Jubb, Z. Sondka, D. M. Beare, N. Bindal, H. Boutselakis, C. G. Cole, C. Creatore, E. Dawson, P. Fish, B. Harsha, C. Hathaway, S. C. Jupe, C. Y. Kok, K. Noble, L. Ponting, C. C. Ramshaw, C. E. Rye, H. E. Speedy, R. Stefancsik, S. L. Thompson, S. Wang, S. Ward, P. J. Campbell, S. A. Forbes, COSMIC: The Catalogue Of Somatic Mutations In Cancer. *Nucleic Acids Res*. **47** (2019), doi:10.1093/nar/gky1015.

42. M. Cordenonsi, F. Zanconato, L. Azzolin, M. Forcato, A. Rosato, C. Frasson, M. Inui, M. Montagner, A. R. Parenti, A. Poletti, M. G. Daidone, S. Dupont, G. Basso, S. Bicciato, S. Piccolo, The hippo transducer TAZ confers cancer stem cell-related traits on breast cancer cells. *Cell*. **147** (2011), doi:10.1016/j.cell.2011.09.048.

43. S. Piccolo, S. Dupont, M. Cordenonsi, The biology of YAP/TAZ: Hippo signaling and beyond. *Physiol Rev*. **94** (2014), doi:10.1152/physrev.00005.2014.

44. P. C. Calses, J. J. Crawford, J. R. Lill, A. Dey, Hippo Pathway in Cancer: Aberrant Regulation and Therapeutic Opportunities. *Trends Cancer*. **5** (2019), , doi:10.1016/j.trecan.2019.04.001.

45. M. L. Fisher, D. Grun, G. Adhikary, W. Xu, R. L. Eckert, Inhibition of YAP function overcomes BRAF inhibitor resistance in melanoma cancer stem cells. *Oncotarget*. **8** (2017), doi:10.18632/oncotarget.22628.

46. A. Kapoor, W. Yao, H. Ying, S. Hua, A. Liewen, Q. Wang, Y. Zhong, C. J. Wu, A. Sadanandam, B. Hu, Q. Chang, G. C. Chu, R. Al-Khalil, S. Jiang, H. Xia, E. Fletcher-Sananikone, C. Lim, G. I. Horwitz, A. Viale, P. Pettazzoni, N. Sanchez, H. Wang, A. Protopopov, J. Zhang, T. Heffernan, R. L. Johnson, L. Chin, Y. A. Wang, G. Draetta, R. A. Depinho, Yap1 activation enables bypass of oncogenic KRAS addiction in pancreatic cancer. *Cell*. **158** (2014), doi:10.1016/j.cell.2014.06.003.

47. M. H. Kim, J. Kim, H. Hong, S. Lee, J. Lee, E. Jung, J. Kim, Actin remodeling confers BRAF inhibitor resistance to melanoma cells through YAP / TAZ activation . *EMBO J*. **35** (2016), doi:10.15252/embj.201592081.

48. S. Kitajima, H. Asahina, T. Chen, S. Guo, L. G. Quiceno, J. D. Cavanaugh, A. A. Merlino, S. Tange, H. Terai, J. W. Kim, X. Wang, S. Zhou, M. Xu, S. Wang, Z. Zhu, T. C. Thai, C. Takahashi, Y. Wang, R. Neve, S. Stinson, P. Tamayo, H. Watanabe, P. T. Kirschmeier, K. K. Wong, D. A. Barbie, Overcoming Resistance to Dual Innate Immune and MEK Inhibition Downstream of KRAS. *Cancer Cell*. **34** (2018), doi:10.1016/j.ccell.2018.08.009.

49. L. Lin, T. G. Bivona, The Hippo effector YAP regulates the response of cancer cells to MAPK pathway inhibitors. *Mol Cell Oncol*. **3** (2016), doi:10.1080/23723556.2015.1021441.

50. D. D. Shao, W. Xue, E. B. Krall, A. Bhutkar, F. Piccioni, X. Wang, A. C. Schinzel, S. Sood, J. Rosenbluh, J. W. Kim, Y. Zwang, T. M. Roberts, D. E. Root, T. Jacks, W. C. Hahn, KRAS and YAP1 converge to regulate EMT and tumor survival. *Cell*. **158** (2014), doi:10.1016/j.cell.2014.06.004.

51. W. Zhao, M. Wang, M. Cai, C. Zhang, Y. Qiu, X. Wang, T. Zhang, H. Zhou, J. Wang, W. Zhao, R. Shao, Transcriptional co-activators YAP/TAZ: Potential therapeutic targets for metastatic breast cancer. *Biomedicine and Pharmacotherapy*. **133** (2021), , doi:10.1016/j.biopha.2020.110956.

52. G. Nardone, J. Oliver-De La Cruz, J. Vrbsky, C. Martini, J. Pribyl, P. Skládal, M. Pešl, G. Caluori, S. Pagliari, F. Martino, Z. Maceckova, M. Hajduch, A. Sanz-Garcia, N. M. Pugno, G. B. Stokin, G. Forte, YAP regulates cell mechanics by controlling focal adhesion assembly. *Nat Commun*. **8** (2017), doi:10.1038/ncomms15321.

53. A. Elosegui-Artola, I. Andreu, A. E. M. Beedle, A. Lezamiz, M. Uroz, A. J. Kosmalska, R. Oria, J. Z. Kechagia, P. Rico-Lastres, A. L. le Roux, C. M. Shanahan, X. Trepat, D. Navajas, S. Garcia-Manyes, P. Roca-Cusachs, Force

Triggers YAP Nuclear Entry by Regulating Transport across Nuclear Pores. *Cell*. **171** (2017), doi:10.1016/j.cell.2017.10.008.

54. B. Zhao, L. Li, K. Tumaneng, C. Y. Wang, K. L. Guan, A coordinated phosphorylation by Lats and CK1 regulates YAP stability through SCFβ-TRCP. *Genes Dev*. **24** (2010), doi:10.1101/gad.1843810.

55. B. Zhang, A. Gong, H. Shi, Q. Bie, Z. Liang, P. Wu, F. Mao, H. Qian, W. Xu, Identification of a novel YAP–14-3-3ζ negative feedback loop in gastric cancer. *Oncotarget*. **8** (2017), doi:10.18632/oncotarget.18011.

56. K. C. Su, T. Takaki, M. Petronczki, Targeting of the RhoGEF Ect2 to the Equatorial Membrane Controls Cleavage Furrow Formation during Cytokinesis. *Dev Cell*. **21** (2011), doi:10.1016/j.devcel.2011.11.003.

57. F. Zanconato, G. Battilana, M. Cordenonsi, S. Piccolo, YAP/TAZ as therapeutic targets in cancer. *Curr Opin Pharmacol*. **29** (2016), , doi:10.1016/j.coph.2016.05.002.

58. C. D. K. Nguyen, C. Yi, YAP/TAZ Signaling and Resistance to Cancer Therapy. *Trends Cancer*. **5** (2019), , doi:10.1016/j.trecan.2019.02.010.

59. T. Moroishi, H. W. Park, B. Qin, Q. Chen, Z. Meng, S. W. Plouffe, K. Taniguchi, F. X. Yu, M. Karin, D. Pan, K. L. Guan, A YAP/TAZ-induced feedback mechanism regulates Hippo pathway homeostasis. *Genes Dev*. **29** (2015), doi:10.1101/gad.262816.115.

60. L. Goentoro, O. Shoval, M. W. Kirschner, U. Alon, The Incoherent Feedforward Loop Can Provide Fold-Change Detection in Gene Regulation. *Mol Cell*. **36** (2009), doi:10.1016/j.molcel.2009.11.018.

61. C. Cohen-Saidon, A. A. Cohen, A. Sigal, Y. Liron, U. Alon, Dynamics and Variability of ERK2 Response to EGF in Individual Living Cells. *Mol Cell*. **36** (2009), doi:10.1016/j.molcel.2009.11.025.

62. L. Goentoro, M. W. Kirschner, Evidence that Fold-Change, and Not Absolute Level, of β-Catenin Dictates Wnt Signaling. *Mol Cell*. **36** (2009), doi:10.1016/j.molcel.2009.11.017.

63. T. Liu, L. Zhou, K. Yang, K. Iwasawa, A. L. Kadekaro, T. Takebe, T. Andl, Y. Zhang, The β-catenin/YAP signaling axis is a key regulator of melanoma-associated fibroblasts. *Signal Transduct Target Ther*. **4** (2019), doi:10.1038/s41392-019-0100-7.

64. J. Rosenbluh, D. Nijhawan, A. G. Cox, X. Li, J. T. Neal, E. J. Schafer, T. I. Zack, X. Wang, A. Tsherniak, A. C. Schinzel, D. D. Shao, S. E. Schumacher, B. A. Weir, F. Vazquez, G. S. Cowley, D. E. Root, J. P. Mesirov, R. Beroukhim, C. J. Kuo, W. Goessling, W. C. Hahn, β-Catenin-driven cancers require a

YAP1 transcriptional complex for survival and tumorigenesis. *Cell*. **151** (2012), doi:10.1016/j.cell.2012.11.026.

Figure Legends:

Figure 1: YAP/TAZ concentration decreases with increasing cell size. A) Log-log plots relating YAP/TAZ and Actin concentration to single-cell area. Assuming a power-law relationship between protein concentration and cell size, the gradient represents the power to which concentration scales with area and the y-intercept determines the maximum concentration. The shaded area denotes one standard deviation of the cell size distribution about that size bin. B) The relationship between YAP/TAZ and actin integrated intensity (proportional to abundance) and single-cell area. Both abundances scale positively with area indicating that both are continually produced. C) Mean YAP/TAZ concentration plotted against mean cell area; while a function of area within a cell line, YAP concentration does not correlate with area across lines ($R = -0.15$, $n = 9$, $P > 0.05$). D) Log-log plots relating YAP/TAZ concentration to single-cell area across DNA bins (blue the least DNA, red, green, yellow the most). Cell membership to each 'bin' was determined by kmeans clustering on the DNA content. The shaded area denotes one standard deviation of the cell size distribution about that size bin. E) Log-log plots relating Actin concentration to single-cell area across DNA bins (blue the least DNA, red, green, yellow the most). Cell membership to each 'bin' was determined by kmeans clustering on the DNA content. YAP/TAZ-size scaling is sensitive to DNA content while Actin scaling, is not. The shaded area denotes one standard deviation of the cell size distribution about that size bin.

Figure 2: YAP/TAZ scaling rate is a function of cell size: A) The relationship between Log(cell area) and the logarithmic derivative of YAP concentration with respect to area. The blue line represents G1 cells, whilst the red represents G2 cells. G1 and G2 groups were determined through kmeans clustering on the integrated Hoechst intensity. Shaded regions represent one standard deviation of all values within the local size 'bin'. B) Average scaling factors within one standard deviation of the G1 area distribution mean. Error bars represent one standard deviation of the scaling factor distribution in that size range. Cell lines marked with an asterisk are those that showed the highest variance in scaling factor within a 'typical' size range, in each case, these cell lines show a larger than average scaling factor at small sizes. C) Average scaling factors within one standard deviation of the G2 area

distribution mean. Error bars represent one standard deviation of the scaling factor distribution in that size range. D) The fold-change between G2 and G1 YAP/TAZ as a function of cell size. The shaded region represents one standard deviation from the mean.

Figure 3: YAP/TAZ nuclear/cytoplasmic ratio behaves oppositely to concentration A) Log-log plots relating YAP/TAZ nuclear-cytoplasm ratios and single cell area across lines and each DNA content bin (as determined by kmeans clustering on the integrated Hoechst intensity and nuclear area). Blue represents the lowest DNA content, then red, green and yellow, the most. The cell line marked with the asterisk is enlarged on the right as an exemplar cell line. In all cases, YAP/TAZ ratio positively scales with cell area but decreases with increasing DNA content. The shaded area denotes one standard deviation of the cell size distribution about that size bin. B) Log-log plots relating nuclear YAP/TAZ single cell nuclear areas across cell lines and DNA contents. The shaded area denotes one standard deviation of the cell size distribution about that size bin. C) Nuclear YAP/TAZ, single cell area relationship plotted across DNA content bins for each cell line. The shaded area denotes one standard deviation of the cell size distribution about that size bin. D) Logarithmic derivatives of nuclear YAP/YAZ concentration per nuclear area showing an exceptionally strong scaling factor at smaller nuclear sizes. The shaded area denotes one standard deviation of the cell size distribution about that size bin. E) Logarithmic derivatives of nuclear YAP/YAZ concentration per cell area. The shaded area denotes one standard deviation of the cell size distribution about that size bin.

Figure 4: Nuclear translocation of YAP/TAZ correlates with a reduction in YAP/TAZ scaling factor. A) Relationship between total YAP/TAZ scaling factor, ‘b’, and cell area (blue) in the G1 cell population (as determined by kmeans clustering on the integrated Hoechst intensity). Cell lines shown are those which exhibited the greatest area sensitivity in their scaling factors. The error margin corresponds to 1 standard deviation in that size bin. The red line is an estimate of ‘b’ assuming a linear relationship between ‘b’ and log(Yn), where Yn is the nuclear YAP/TAZ concentration. B) YAP/TAZ nuc/cyto ratio against the average cytoplasmic YAP/TAZ

scaling factor. A significant difference in population scaling factor means was detected across either side of the mean YAP/TAZ ratio (T-Test, n = 4, 5, P <0.0001, each mean calculated from 2000 – 5000 cells depending on cell line). C) Nuclear YAP/TAZ concentration against the average cytoplasmic YAP/TAZ scaling factor. No clear relationship was observed across cell lines.

Figure 5: YAP/TAZ scaling behaviour is consistent with a dilution-synthesis-dilution scheme. A) Schematic describing the logic of the dilution-synthesis-dilution system. Relevant dilution factors are marked on each stage. The colours correspond to the final concentration at the end of the stage. Blue is low, orange high. B) Model fits on the single cell G2 (as determined by kmeans clustering on the integrated Hoechst intensity) size distributions, blue represents experimental data, orange is the calculated distribution and yellow is the Kullbeck-Leibler Divergence between the distributions. C) The dilution factor probability distribution (P(D)) across a range of scaling factors. D) The dilution factor product probability distribution F(z) across a range of scaling factors. E) The relationship between the coefficient of variation and the mean of F(z). The CV increases as the mean decreases. F) Schematic describing how the dilution factor distribution P(D) is used to calculate the expected YAP/TAZ concentration distribution G) Measured YAP/TAZ intensity distributions (blue) and the associated model fits (orange). In all cases we observe excellent agreement.

Figure 6: YAP/TAZ scaling behaviour drives increasing nuclear/cytoplasmic ratios under a range of genetic perturbations: A) Log-log plots showing the scaling relationships between cell area and YAP/TAZ concentration (left) and nuclear concentration (right) across LATS1/2 knockdown states. The colour denotes DNA content clusters as determined by kmeans on the integrated Hoescht intensity. The shaded area denotes one standard deviation of the cell size distribution about that size bin. B(top left)) The relationship between the squared YAP/TAZ concentration (Z-score) and squared model error (Z-score) for each knockdown state in LM2 cells. The colour and size of each datapoint corresponds to the distance from the origin. B(bottom left)) The relationship between the squared YAP/TAZ concentration (Z-

score) and squared model error (Z-score) for each knockdown state in M231 cells. The colour and size of each datapoint corresponds to the distance from the origin. Inset: zoom in on the red marked region. We note a strong overlap in hits across the two cell lines. B(top right)) The relationship between the squared YAP/TAZ ratio and squared model error for each knockdown state in LM2 cells. KDs affecting YAP/TAZ ratio are not redundant with those affecting concentration. The colour and size of each datapoint corresponds to the distance from the origin. Inset: zoom in on the red marked region. B(bottom right)) The relationship between the squared YAP/TAZ ratio and squared model error for each knockdown state in M231 cells. The colour and size of each datapoint corresponds to the distance from the origin. Inset: zoom in on the red marked region. C) Comparisons of YAP/TAZ concentration, YAP/TAZ nuclear concentration, YAP/TAZ N/C ratio and cell area across knockdown states by an N-way ANOVA test (n = 200 for control, 4 for all else, ** denotes $P < 0.01$).

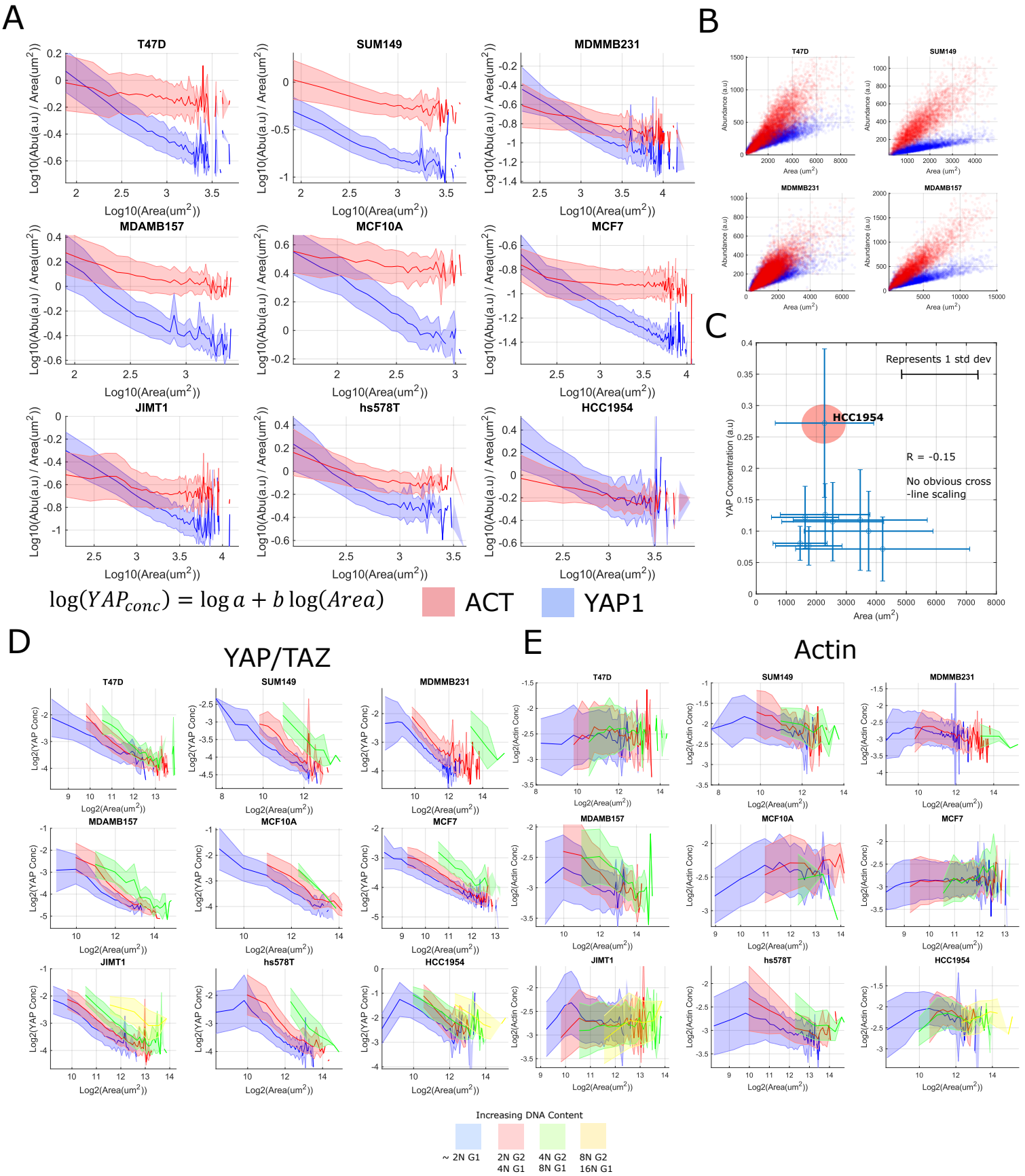
A
T47D
SUM149
MDMMB231
MDAMB157
MCF10A
MCF7
JIMT1
hs578T
HCC1954
Log10(Abu(a.u) / Area(um2))
Log10(Area(um2))
$\log(YAP_{conc}) = \log a + b \log(Area)$
ACT
YAP1
B
Abundance (a.u)
Area (um2)
C
Represents 1 std dev
HCC1954
R = -0.15
No obvious cross
-line scaling
YAP Concentration (a.u)
Area (um2)
D
YAP/TAZ
Log2(YAP Conc)
Log2(Area(um2))
E
Actin
Log2(Actin Conc)
Log2(Area(um2))
Increasing DNA Content
~ 2N G1
2N G2
4N G1
4N G2
8N G1
8N G2
16N G1

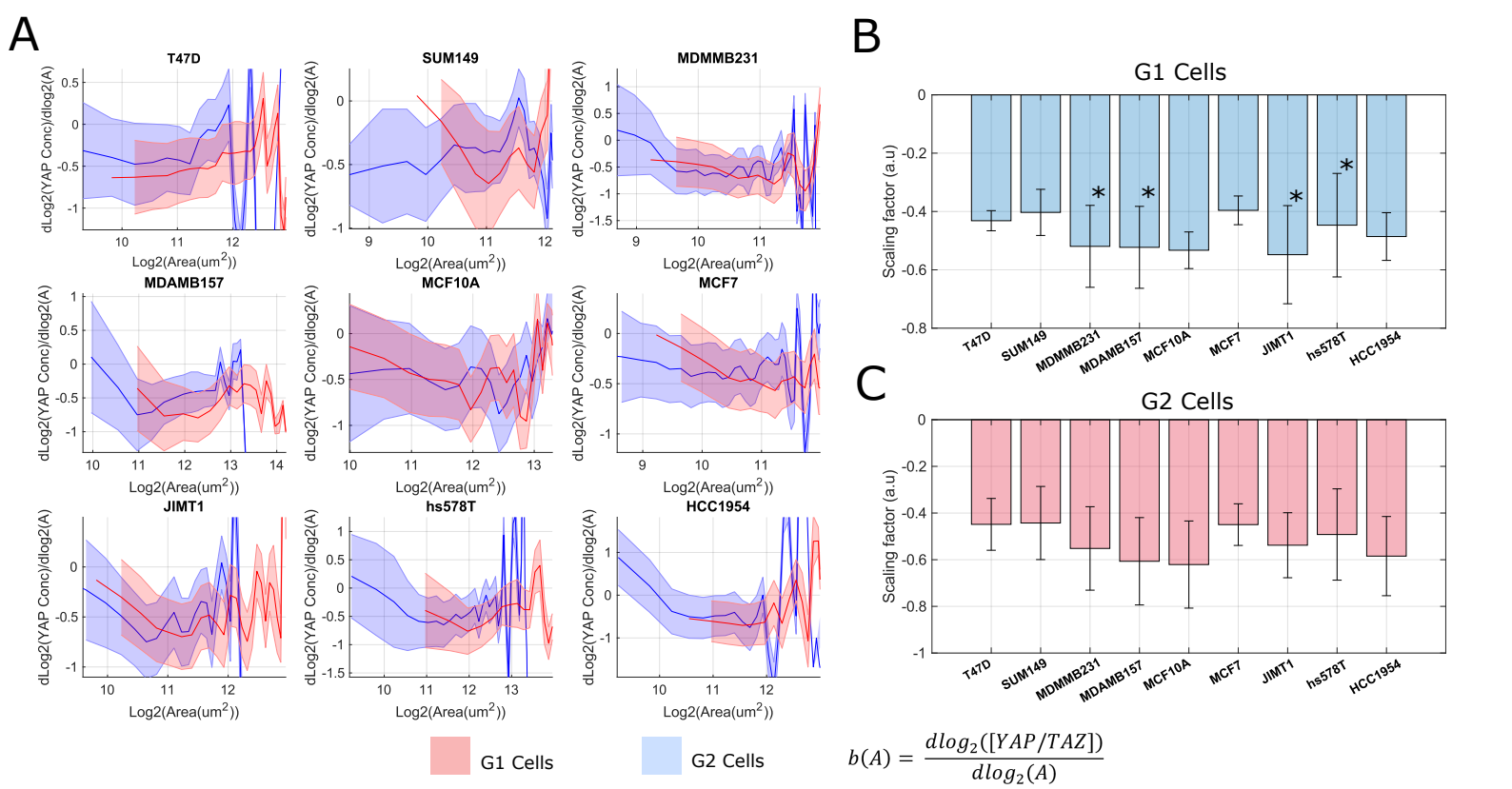

$$b(A) = \frac{dlog_2([YAP/TAZ])}{dlog_2(A)}$$

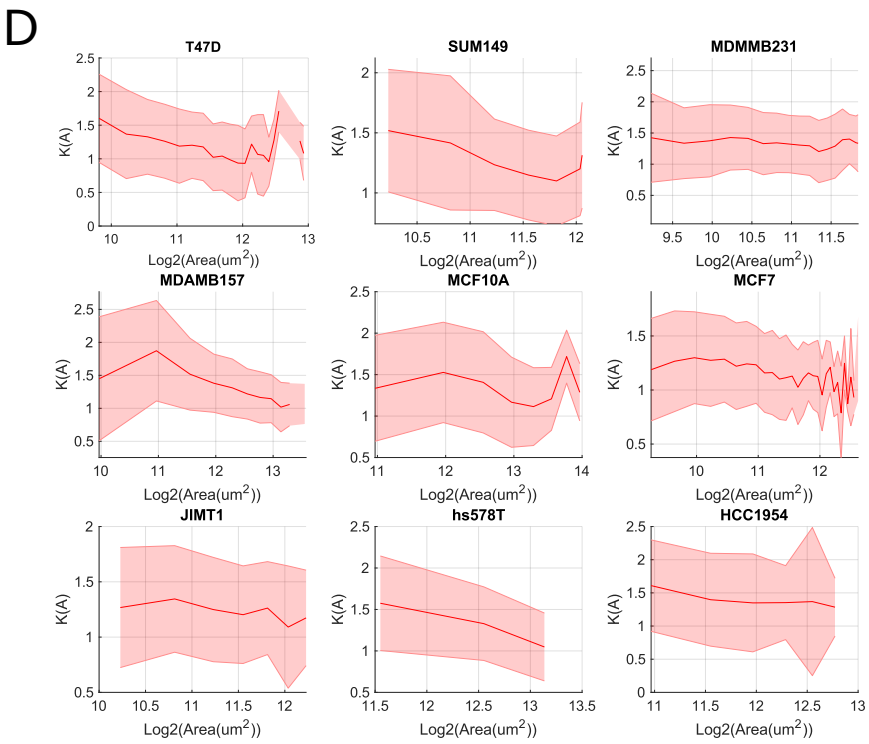

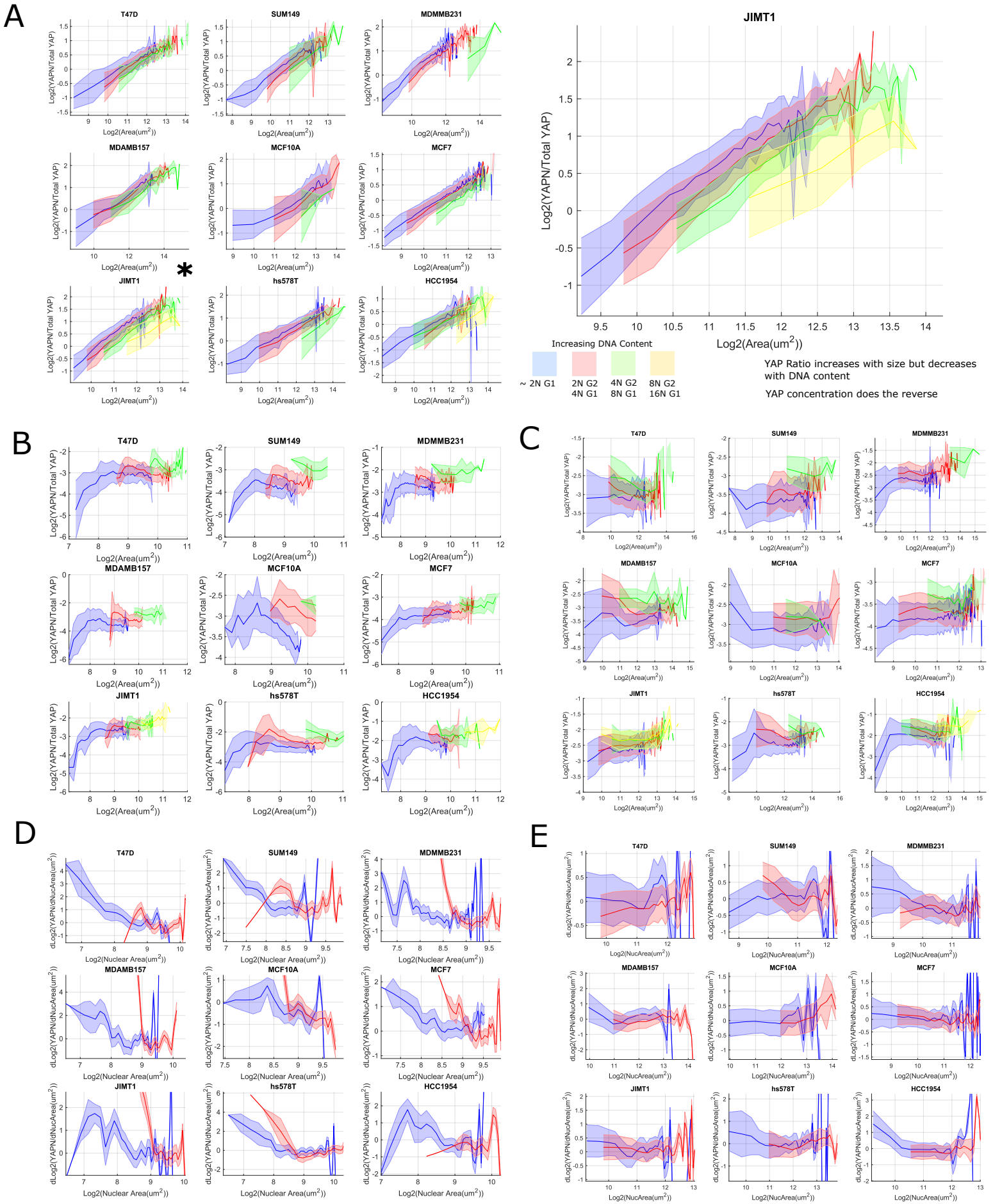
A
T47D
SUM149
MDMMB231
MDAMB157
MCF10A
MCF7
JIMT1
hs578T
HCC1954
Log2(YAPN/Total YAP)
Log2(Area(um2))
*
JIMT1
Log2(YAPN/Total YAP)
Log2(Area(um2))
Increasing DNA Content
~ 2N G1
2N G2
4N G1
4N G2
8N G1
8N G2
16N G1
YAP Ratio increases with size but decreases with DNA content
YAP concentration does the reverse
B
C
D
dLog2(YAPN/dNucArea(um2))
Log2(Nuclear Area(um2))
E
Log2(NucArea(um2))

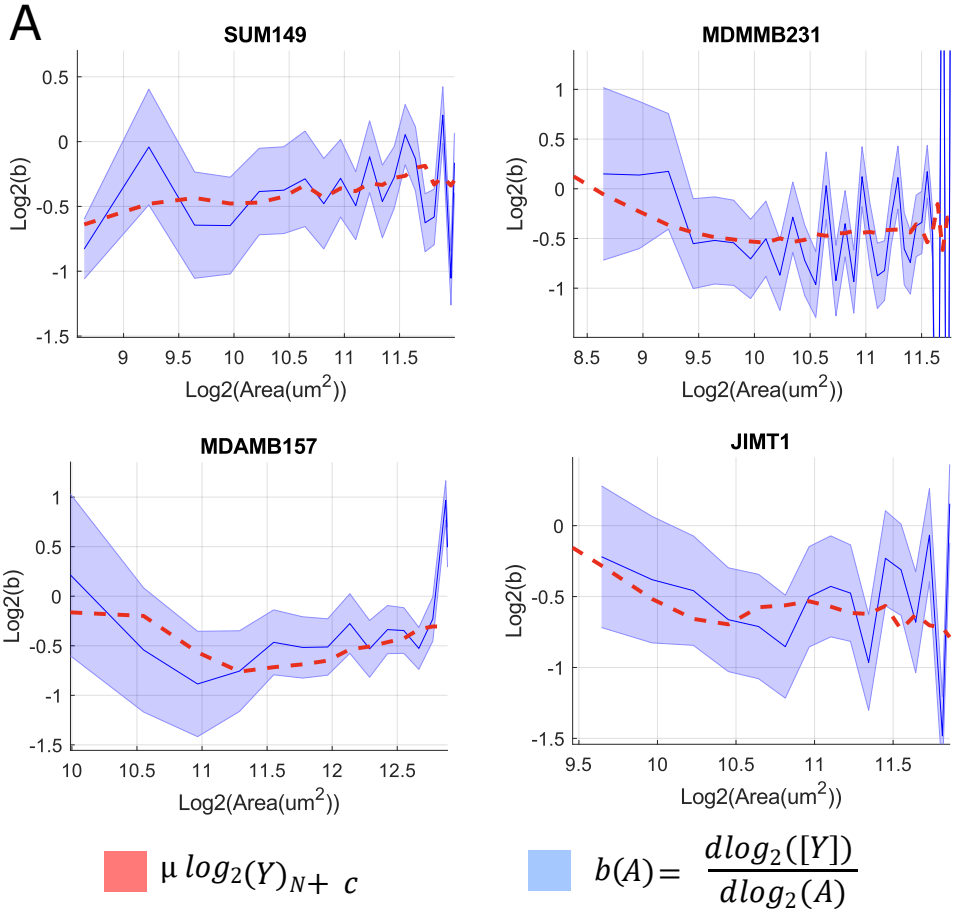
A
SUM149
MDMMB231
MDAMB157
JIMT1
Log2(b)
Log2(Area(um^2))
μ $log_2(Y)_N + c$
$b(A) = \frac{dlog_2([Y])}{dlog_2(A)}$

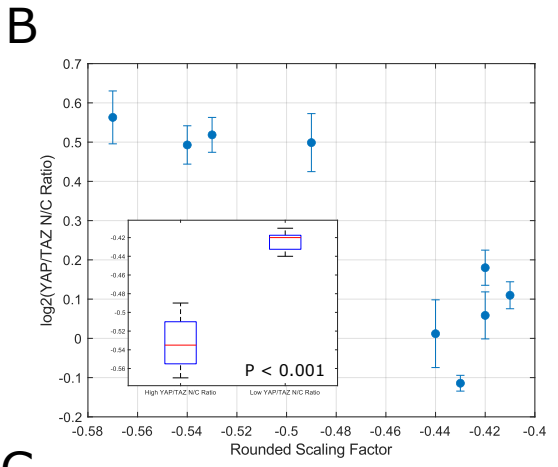
B
log2(YAP/TAZ N/C Ratio)
Rounded Scaling Factor
P < 0.001
High YAP/TAZ N/C Ratio
Low YAP/TAZ N/C Ratio

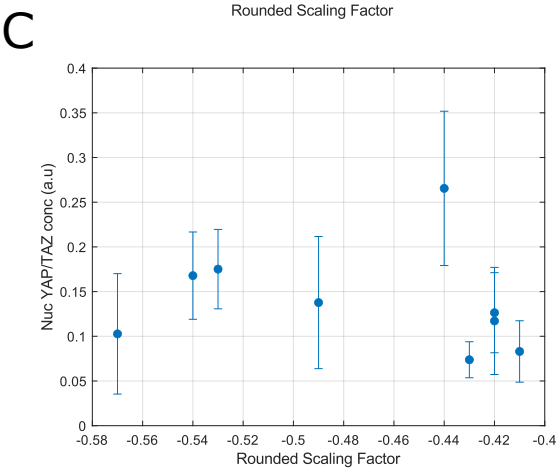
C
Nuc YAP/TAZ conc (a.u)
Rounded Scaling Factor

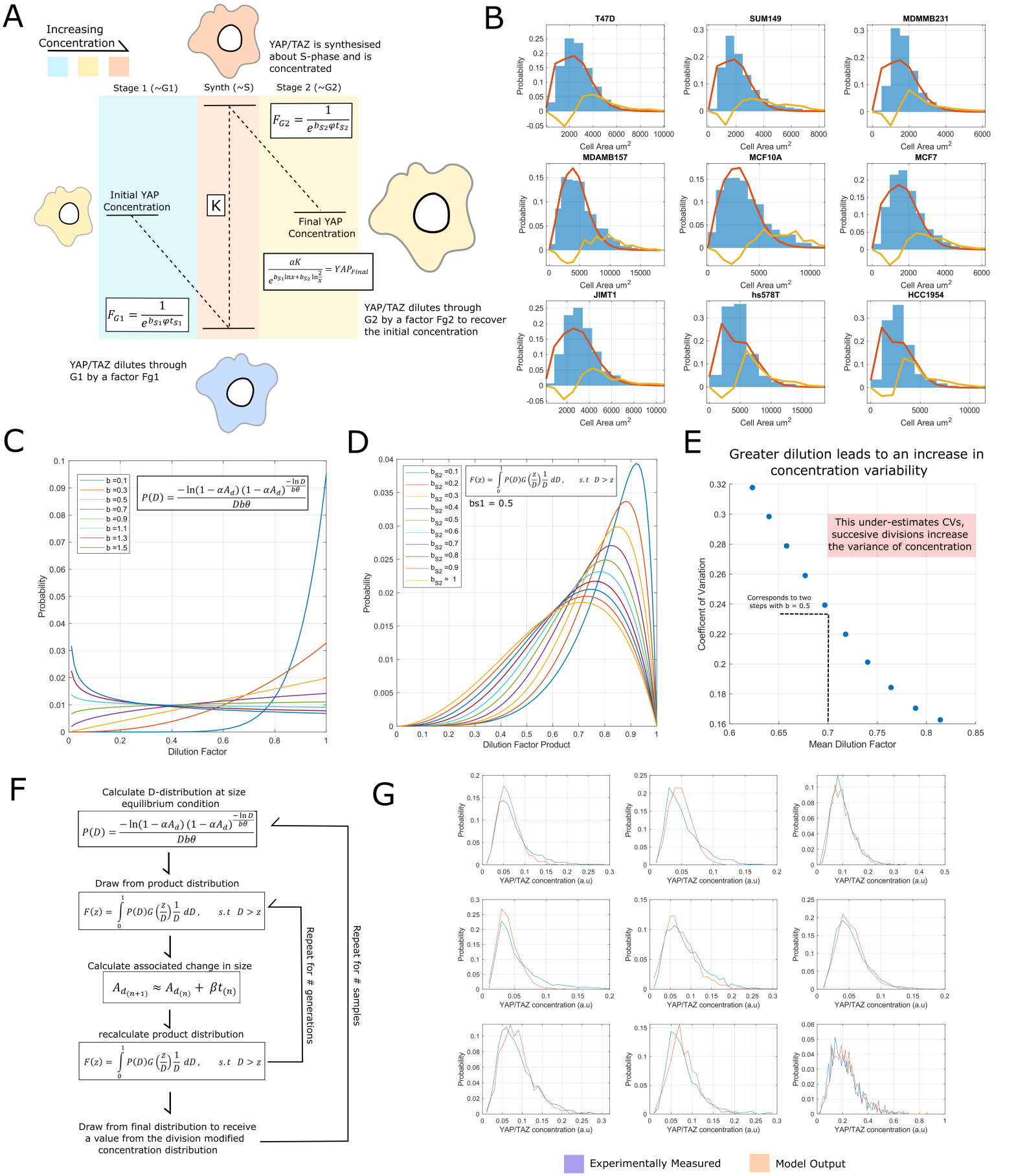
A
Increasing Concentration
YAP/TAZ is synthesised about S-phase and is concentrated
Stage 1 (~G1)
Synth (~S)
Stage 2 (~G2)
$F_{G2} = \frac{1}{e^{b_{S2}\varphi t_{S2}}}$
Initial YAP Concentration
K
Final YAP Concentration
$\frac{aK}{e^{b_{S1}\ln x + b_{S2}\ln\frac{2}{x}}} = YAP_{Final}$
$F_{G1} = \frac{1}{e^{b_{S1}\varphi t_{S1}}}$
YAP/TAZ dilutes through G2 by a factor Fg2 to recover the initial concentration
YAP/TAZ dilutes through G1 by a factor Fg1
B
T47D
SUM149
MDMMB231
MDAMB157
MCF10A
MCF7
JIMT1
hs578T
HCC1954
Probability
Cell Area um^2
C
$P(D) = \frac{-\ln(1-\alpha A_d)(1-\alpha A_d)^{\frac{-\ln D}{b\theta}}}{Db\theta}$
b =0.1
b =0.3
b =0.5
b =0.7
b =0.9
b =1.1
b =1.3
b =1.5
Probability
Dilution Factor
D
$F(z) = \int_0^1 P(D)G\left(\frac{z}{D}\right)\frac{1}{D}\,dD, \quad s.t\ D > z$
bs1 = 0.5
b_{S2} =0.1
b_{S2} =0.2
b_{S2} =0.3
b_{S2} =0.4
b_{S2} =0.5
b_{S2} =0.6
b_{S2} =0.7
b_{S2} =0.8
b_{S2} =0.9
b_{S2} = 1
Probability
Dilution Factor Product
E
Greater dilution leads to an increase in concentration variability
This under-estimates CVs, succesive divisions increase the variance of concentration
Corresponds to two steps with b = 0.5
Coefficent of Variation
Mean Dilution Factor
F
Calculate D-distribution at size equilibrium condition
$P(D) = \frac{-\ln(1-\alpha A_d)(1-\alpha A_d)^{\frac{-\ln D}{b\theta}}}{Db\theta}$
Draw from product distribution
$F(z) = \int_0^1 P(D)G\left(\frac{z}{D}\right)\frac{1}{D}\,dD, \quad s.t\ D > z$
Calculate associated change in size
$A_{d_{(n+1)}} \approx A_{d_{(n)}} + \beta t_{(n)}$
recalculate product distribution
$F(z) = \int_0^1 P(D)G\left(\frac{z}{D}\right)\frac{1}{D}\,dD, \quad s.t\ D > z$
Draw from final distribution to receive a value from the division modified concentration distribution
Repeat for # generations
Repeat for # samples
G
Probability
YAP/TAZ concentration (a.u)
Experimentally Measured
Model Output

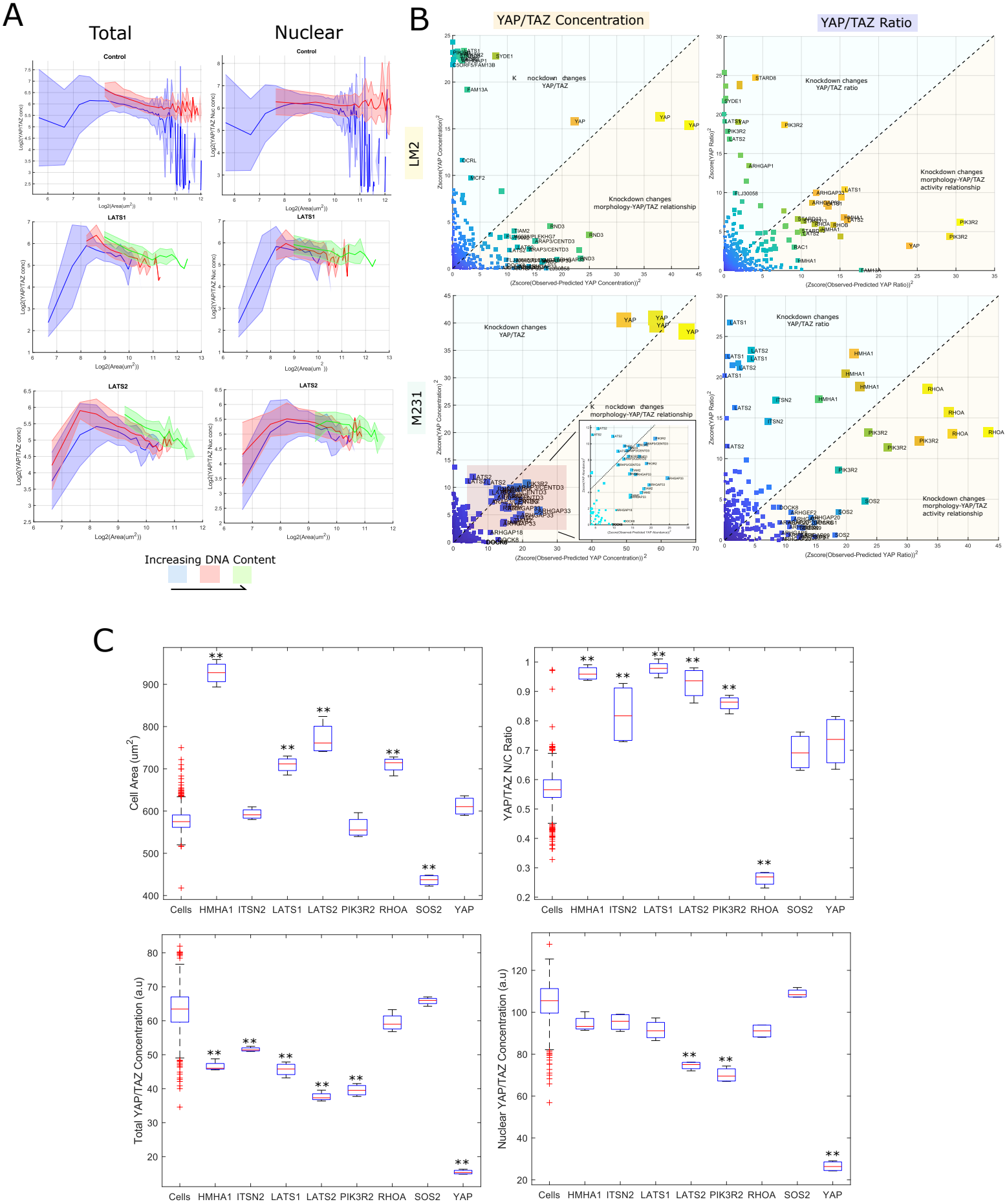
A
Total
Nuclear
Control
LATS1
LATS2
Log2(Area(um^2))
Log2(YAP/TAZ conc)
Log2(YAP/TAZ Nuc conc)
Increasing DNA Content
B
YAP/TAZ Concentration
YAP/TAZ Ratio
LM2
M231
Knockdown changes YAP/TAZ
Knockdown changes morphology-YAP/TAZ relationship
Knockdown changes YAP/TAZ ratio
Knockdown changes morphology-YAP/TAZ activity relationship
Zscore(YAP Concentration)^2
Zscore(YAP Ratio)^2
(Zscore(Observed-Predicted YAP Concentration))^2
(Zscore(Observed-Predicted YAP Ratio))^2
C
Cell Area (um^2)
YAP/TAZ N/C Ratio
Total YAP/TAZ Concentration (a.u)
Nuclear YAP/TAZ Concentration (a.u)
Cells
HMHA1
ITSN2
LATS1
LATS2
PIK3R2
RHOA
SOS2
YAP